NASA TECHNICAL NOTE

NASA TN D-7665

NASA TN D-7665

(NASA-TN-D-7665) CRACK-GROWTH BEHAVIOR IN THICK WELDED PLATES OF INCONEL 718 AT RCCM AND CRYOGENIC TEMPERATURES (NASA) 50 p HC $3.25 CSCL 11F

N74-23116

Unclas H1/17 39128

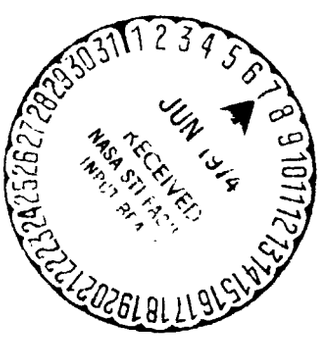

CRACK-GROWTH BEHAVIOR IN THICK WELDED PLATES OF INCONEL 718 AT ROOM AND CRYOGENIC TEMPERATURES

by Royce G. Forman

Lyndon B. Johnson Space Center
Houston, Texas 77058

NATIONAL AERONAUTICS AND SPACE ADMINISTRATION • WASHINGTON, D. C. • MAY 1974

1 Report No	2 Government Accession No	3 Recipient's Catalog No
NASA TN D-7665		

4 Title and Subtitle	5 Report Date
CRACK-GROWTH BEHAVIOR IN THICK WELDED PLATES OF INCONEL 718 AT ROOM AND CRYOGENIC TEMPERATURES	May 1974
	6 Performing Organization Code
7 Author(s)	8 Performing Organization Report No
Royce G. Forman, JSC	JSC S-391
	10 Work Unit No
9 Performing Organization Name and Address	968-15-11-01-72
Lyndon B. Johnson Space Center Houston, Texas 77058	11 Contract or Grant No
	13 Type of Report and Period Covered
12 Sponsoring Agency Name and Address	Technical Note
National Aeronautics and Space Administration Washington, D.C. 20546	14 Sponsoring Agency Code

15 Supplementary Notes

16 Abstract

Results of mechanical-properties and axial-load fatigue and fracture tests performed on thick welded plates of Inconel 718 superalloy are presented. The test objectives were to determine the tensile strength properties and the crack-growth behavior in electron-beam, plasma-arc, and gas tungsten arc welds for plates 1.90 centimeters (0.75 inch) thick. Base-metal specimens were also tested to determine the flaw-growth behavior. The tests were performed in room-temperature-air and liquid nitrogen environments. The experimental crack-growth-rate data are correlated with theoretical crack-growth-rate predictions for semielliptical surface flaws.

17. Key Words (Suggested by Author(s))		18. Distribution Statement
*Electron Beam Welding	*Fatigue Tests	STAR Subject Category: 17
*Gas Tungsten Arc Welding	*Weld Strength	
*Plasma Arc Welding	*Tensile Strength	
*Fracture Toughness	*Heat Treatment	
*Heat Resistant Alloy	*Aging	

19 Security Classif. (of this report)	20 Security Classif. (of this page)	21. No. of Pages	22 Price
None	None	48	$3.25

* For sale by the National Technical Information Service, Springfield, Virginia 22151

CONTENTS

PRECEDING PAGE BLANK NOT FILMED

TABLES

FIGURES

CRACK-GROWTH BEHAVIOR IN THICK WELDED PLATES OF INCONEL 718 AT ROOM AND CRYOGENIC TEMPERATURES

By Royce G. Forman
Lyndon B. Johnson Space Center

SUMMARY

Smooth tensile specimens and surface-cracked fatigue and fracture specimens from 1.90-centimeter (0.75 inch) thick Inconel 718 plate were tested to determine mechanical properties and crack-growth behavior. Base metal and four types of welds were tested in environments of ambient air and liquid nitrogen. Of the different types of welds, more difficulty was encountered in producing acceptable welds using the electron-beam and plasma-arc processes. Also, these welds exhibited lower fracture-toughness properties and higher crack-growth rates than the two different types of gas tungsten arc welds. Base-metal results showed significantly higher fracture-toughness and lower crack-growth-rate properties than corresponding properties for any of the weld processes. The crack-growth-rate experimental results showed correlation with theoretical results for both base metal and weld metal.

INTRODUCTION

One of the many alternatives considered for the first stage of the Space Shuttle vehicle was a pressure-fed booster containing liquid oxygen and liquid propane propellants. The large diameter of 8.2 meters (27 feet) and the high internal tank pressure of 2.76 MN/m^2 (400 psi) necessitated tanks having walls thicker than any previously built for space application. A fabrication feasibility assessment was therefore undertaken at the NASA Lyndon B. Johnson Space Center (JSC) for three materials: 2219-T87 aluminum alloy, Inconel 718, and 200 grade maraging steel. The investigation included preliminary assessments concerning potential problems in the areas of welding, forging, machining, roll forming, heat treatment, corrosion, fracture toughness, and mechanical properties.

From the assessment, it was found that data were almost completely lacking in the areas of fracture toughness, fatigue-crack-growth rates, and mechanical properties of thick welds in the three materials. These data were necessary to determine weldland dimensions, to determine flaw-detection requirements, and to estimate proof-test requirements for preventing failures at operating pressure levels. To obtain these data, tests were first performed on thick welded plates of 2219-T87 aluminum alloy. These results are discussed in reference 1. The subsequent testing on thick plates of

Inconel 718 is discussed in this report. The testing of 200 grade maraging steel was not made part of the NASA program because a Space Shuttle study contractor was independently obtaining these data.

The experimental results obtained for Inconel 718 were for base metal and four different types of welds. The four weld techniques evaluated were as follows:

1. Electron beam (EB)
2. Gas tungsten arc (GTA)
3. Pulse-current gas tungsten arc (pulse GTA)
4. Plasma-arc root weld with gas tungsten arc fill passes (PAW-GTA)

Except for some of the GTA weld specimens, all base-metal and weld-metal specimens had a 991 K (1325° F) aging heat treatment before final machining. The GTA weld specimens were tested after being given one of three different heat treatments. The test environments used in the program were room-temperature air and liquid nitrogen (LN_2). All welds were perpendicular to the longitudinal (loaded) axis of the specimens.

As an aid to the reader, where necessary the original units of measure have been converted to the equivalent value in the Système International d'Unités (SI). The SI units are written first, and the original units are written parenthetically thereafter.

SYMBOLS

The SI unit conversion factors used with these symbols are listed in the appendix.

a crack depth, centimeters (inches)

b crack half-length, centimeters (inches)

C_a material constant for crack growth in the a direction

C_b material constant for crack growth in the b direction

E modulus of elasticity, GN/m^2 (ksi)

F correction factor for the effect of the cracked plate surface (front face) on the growth of a crack through the thickness

F_{TU} ultimate tensile strength, MN/m^2 (ksi)

F_{TY} tensile yield strength (0.2-percent offset), MN/m^2 (ksi)

K stress-intensity factor, $MN/m^{3/2}$ ($ksi\sqrt{in.}$)

K_{IE} critical stress-intensity factor at fracture for surface-flawed specimens, $MN/m^{3/2}$ ($ksi\sqrt{in.}$)

M correction factor for the effect of crack shape and depth on the growth of a crack through the thickness

N number of fatigue load cycles

Q flaw-shape correction factor

R ratio of minimum applied stress to maximum applied stress in a fatigue cycle

r_x crack-tip yield-zone radius on surface of specimen, millimeters (inches)

r_y crack-tip yield-zone radius at point of maximum crack depth, millimeters (inches)

S numerical exponent in the fatigue-crack-growth equation

t plate thickness, millimeters (inches)

w specimen width, millimeters (inches)

ΔK_a stress-intensity-factor range at the minor axis of the semielliptical crack, $MN/m^{3/2}$ ($ksi\sqrt{in.}$)

ΔK_b stress-intensity-factor range at crack tip on surface of specimen during a fatigue cycle, $MN/m^{3/2}$ ($ksi\sqrt{in.}$)

$\Delta\sigma$ stress range during a fatigue cycle, maximum σ minus minimum σ, MN/m^2 (ksi)

θ angular coordinate

σ applied stress, MN/m^2 (ksi)

Φ complete elliptic integral of the second type

Subscripts:

avg. average conditions for N cycles

c conditions at failure

f final conditions after N cycles

i initial conditions before N cycles

TEST SPECIMEN DESCRIPTION

The specimen fabrication for the Inconel 718 program was divided into two phases (Phases I and II), and two contractors (designated contractor X and contractor Y in this report) were used to perform the welding and to assist in other fabrication steps. Phase I of the program consisted of contractor X welding 17 crack-growth specimens and 3 plates for tensile specimens to develop initial weld parameters and test data. The welding was done on material already purchased by contractor X. The majority of specimen preparation and testing was done in Phase II on 62 crack-growth specimens and 19 tensile specimens, most of which were welded by contractor X and the remainder by contractor Y. The Phase II specimens were all obtained from a single heat of material purchased by NASA and shipped to the contractors. Both the Phase I material and the NASA-supplied material consisted of 1.90-centimeter (0.75 inch) thick plate purchased to specification AMS-5596.

All welding in the program was done on the material in the as-received heat-treatment condition. This condition consisted of a 1228 K (1750° F) solution treatment for one-half hour and an air cooling. The chemical analysis and source of the NASA-purchased material are given in table I. No analysis is available for the Phase I material purchased by contractor X.

After welding, all heat treatment and machining were performed either by JSC or by contractor Y, and all testing was performed at JSC. Specific details of the fabrication processes are given in the following subsections.

Welding Processes

The welding processes selected were based on experience and available technology for welding thick Inconel 718 plate material. Contractor X, who did all of the welding for Phase I, selected GTA, EB, and PAW-GTA weld processes for the Phase I program. In Phase II, contractor X selected the GTA process with a different joint configuration and a full-penetration plasma-arc process. Contractor Y selected the pulse GTA process. The weld parameters and joint configurations for these processes are shown in figures 1 to 5. Photographs of the polished and etched weld cross sections are shown in figures 6 to 9.

For the GTA process, the joint design shown in figure 1 was used for welding Phase I specimens. After completing these welds, the contractor decided that a

narrower groove could be used with fewer passes; thus, the joint shown in figure 2 was used for Phase II GTA welds. Other than some isolated cases of lack of fusion and porosity caused partly by malfunctioning of the equipment, no significant problems were found by contractor X in making satisfactory GTA welds with either wide or narrow groove configurations.

The pulse GTA welds made by contractor Y had the joint configuration and weld parameters shown in figure 3. For unknown reasons, which probably involved malfunctioning of the equipment, the pulse GTA welds had an intermittent lack of root penetration. This condition is shown in figure 7, which consists of two photographs of weld cross sections taken at different locations in a single plate. The lack of penetration did not appear to significantly affect the test results.

Electron-beam welding resulted in the greatest number of problems. The initial approach was to use a square groove joint without a backup plate and to make the weld very narrow. This approach resulted in a weld having questionable sidewall fusion as indicated by a cross section showing a very narrow and irregular fusion zone. Widening the weld resulted in sharp-tailed porosity-type indications along the centerline of the weld as determined by radiographic examination. A different approach was then used to permit any entrapped gases to be liberated to the surface of the molten weld before solidification. This approach consisted of slowing the welding travel speed appreciably and providing a much wider weld (0.25 centimeter (0.1 inch)). To contain the molten puddle, a 0.952-centimeter (0.375 inch) thick Inconel 718 backing strip was used. The electron beam did not penetrate through this strip. Radiographic examination of this weld still showed some fuzzy, hairline defect indications along the centerline of the weld. These indications could not be identified by subsequent metallographic examination. Further development in an effort to obtain defect-free welds proved to be fruitless. The finally selected EB weld parameters, which were the same for both Phase I and Phase II specimens, are shown in figure 4. A cross section of an EB weld is shown in figure 8. Examination of microsections of the weldments did not show any general microfissuring; however, some microfissuring was found in the adjacent heat-affected area as shown in figure 8(b).

The PAW-GTA welding was accomplished using the edge prepa and parameters shown in figure 5. The cross section of the weld is shown in f 6(b). This configuration, with a 0.51-centimeter (0.20 inch) thick root land, wa. onsidered acceptable and ensured complete root penetration by plasma-arc welding when the keyhole mode was used without filler wire. The subsequent filler passes were made using GTA instead of PAW because preliminary investigation had indicated that welding subsequent passes by PAW using filler wire resulted in gross porosity tunneling. However, this problem was generally eliminated for the Phase II specimens, for which a different welding facility was used. In the Phase II program, a joint configuration having a thicker (1.27 centimeters (0.50 inch)) root land was developed after initial work indicated that it could be penetrated by a plasma arc in a single pass. The filler passes, which were made using PAW instead of GTA, were found to be defect-free by radiographic inspection. However, a serious problem with the PAW process in the Phase II program was that the plates had excessive distortion. A cross section of the weld and the excessive plate distortion are shown in the photographs in figure 9. Because of this distortion, none of these specimens were straight enough to machine and, thus, none of these specimens were tested. It should be stated, however, that the distortion resulting from the deep-penetration PAW process might have been satisfactorily minimized with additional development effort.

Machining and Heat Treatment

In the Phase I program, the welded plates used for the surface-flawed specimens were 10 centimeters (4.0 inches) wide, excluding the weld tabs used at the beginning and ends of the welds. For the Phase II welding of NASA material, the plates had approximately 99-centimeter (39 inch) long weld joints. After welding, the plates were cut by plasma arc into cross-weld specimens (welds perpendicular to longitudinal axis) approximately 8.2 centimeters (3.2 inches) wide.

Heat treatment and final machining of the Phase I GTA and PAW-GTA weld specimens were performed by NASA. Heat treatment of all other specimens fabricated for the test program was done by contractor Y. Contractor Y also machined the Phase II GTA and pulse GTA specimens after heat treatment. All other machining of specimens after heat treatment was performed by NASA. A photograph of a surface-flaw weld specimen after heat treatment and a photograph of another specimen after machining flat and notching the starter flaw with an electrical discharge machine are shown in figure 10. Final dimensions for each specimen tested are listed in tables II to IV.

After all welding was complete, the remaining unwelded Phase II plate material was cut into bars approximately 8.9 centimeters (3.5 inches) wide by 41 centimeters (16 inches) long to be used for base-metal tests. The longitudinal grain direction for these specimens was transverse to the loaded direction of the specimens. Heat treatment of the base-metal specimens was performed by contractor Y, and final machining was performed by NASA.

Three different heat treatments after welding were studied in the test program. The first heat treatment, referred to as "A," was the normally recommended 991 K (1325° F) aging treatment. This treatment was used on all welded and base-metal specimens except for some of the Phase II GTA welded material. The two additional heat treatments for this welded material were included to determine the effect of re-solution treatment after welding and the effect of having the aging temperature 55.5 K (100° F) above normal to simulate inadequate temperature control of a very large heat-treatment facility. The three heat-treatment conditions, designated A, B, and C, were as follows.

1. Treatment A - age at 991 K (1325° F) for 8 hours, furnace-cool at 55.5 K (100° F) per hour to 894 K (1150° F), hold for 8 hours, and air-cool.

2. Treatment B - age same as treatment A, re-solution treat at 1228 K (1750° F), and re-age to treatment A.

3. Treatment C - age same as treatment A, re-solution treat at 1228 K (1750° F), re-age at 1047 K (1425° F) for 8 hours, cool to 922 K (1200° F), hold for 8 hours, and air-cool.

Tensile specimens were fabricated and tested for each type of weld and heat treatment. A drawing of a typical tensile specimen is shown in figure 11. For the Phase I material, all tensile specimens for each type weld were machined from the same plate, which was welded specifically for making these specimens. For the Phase II material, the tensile specimens were machined from the same large plates from which the crack-growth specimens were obtained. The heat treatment of tensile specimens and of

corresponding crack-growth specimens for a given type weld was done at the same time in the same furnace. Twelve tensile property specimens were tested in Phase I and 19 in Phase II.

Specimen Prefix Symbols

Prefix letters were used in numbering the crack-growth and tensile specimens to identify the type of weld, the welding contractor and material supplier, and the heat treatment, respectively. Four such letters were used for the crack-growth specimens and three for the tensile specimens. The meaning of the prefix letters is as follows:

Crack-growth specimens	Tensile specimens
First two letters (XX--):	First letter (X--):
GT - GTA weld	G - GTA weld
EB - EB weld	E - EB weld
PA - PAW-GTA weld	P - PAW-GTA weld
BA - base material	B - base material
Third letter (--X-):	Second letter (-X-):
X - contractor X Phase I weld	X - contractor X Phase I weld
N - contractor X Phase II weld	N - contractor X Phase II weld
Y - contractor Y Phase II weld	Y - contractor Y Phase II weld
Fourth letter (---X):	Third letter (--X):
A - heat treatment A	A - heat treatment A
B - heat treatment B	B - heat treatment B
C - heat treatment C	C - heat treatment C

The following table contains a complete list of prefix symbols used and the number of specimens tested for each prefix.

Crack-growth specimen prefix	Number of specimens tested	Tensile specimen prefix	Number of specimens tested
GTXA	5	GXA	2
GTNA	14	GNA	5
GTNB	8	GNB	3
GTNC	6	GNC	3
GTYA	7	GYA	4
EBXA	6	EXA	6
EBNA	8	ENA	2
PAXA	6	PXA	4
BANA	19	BNA	2
Total	79		31

TEST APPARATUS AND PROCEDURES

T .e testing of the Inconel 718 welded and base-metal specimens was performed in air at room temperature and in liquid nitrogen to obtain the following properties.

1. Tensile properties

   a. Ultimate tensile strength F_{TU}

   b. Tensile yield strength (0.2-percent offset) F_{TY}

   c. Modulus of elasticity E

2. Critical stress-intensity factor at fracture for surface-flawed specimens K_{IE}

3. Fatigue-crack-growth rates for surface-type flaws da/dN, where a is the crack depth and N is the number of fatigue load cycles.

All testing of flawed specimens was performed using a 272 000-kilogram (600 000 pound) capacity, hydraulically operated, axial-load fatigue testing machine. The loads were applied through self-alining, hydraulically operated friction grips. The tensile-properties tests were done on a 45 000-kilogram (100 000 pound) capacity tensile testing machine. The cryogenic tests were performed by enclosing the specimens in an open-top polyurethane foam container filled with liquid nitrogen. A soaking time of approximately 20 minutes was required to stabilize a specimen at LN_2 temperature before each test.

To induce all initial fatigue cracks in the surface-flawed specimens, the surfaces were notched using an electrical discharge machine; then cracks were grown from the notches (precracking) by subjecting the specimens to bending fatigue. The machined notches were approximately 1.3 centimeters (0.5 inch) long and 0.25 centimeter (0.1 inch) deep. Precracking was done at a load ratio R of 0.1 and a maximum load such that a fatigue crack 0.25 centimeter (0.1 inch) long developed on each end of the notch in an average of 160 000 cycles. Thus, the growth rate for precracking was very low and was less than any measured in the subsequent growth-rate tests. Therefore, the crack-growth test results were not altered or affected because of high precracking stresses.

Initially, precracked fracture specimens for the base and weld metal were statically tested to failure to obtain preliminary fracture-toughness values. Afterwards, all specimens were axially fatigue cycled at prespecified load levels and number of cycles and then were pulled to failure. By applying fatigue cycles, then pulling to failure, a growth-rate data point was obtained together with a fracture-toughness value for each specimen.

The tensile yield strength properties for the base and weld materials were obtained from strain gages on the tensile specimens. The strain-gage lengths were approximately one-half the width of the welds. The gages were installed back to back on opposite faces of the specimens, and the strain readings were averaged to cancel bending effects.

RESULTS AND DISCUSSION

In this section, results of tensile strength tests, fracture-toughness results, results of fatigue-crack-growth tests, and correlation of experimental and theoretical crack-growth data are presented.

Tensile Strength Tests

Twenty-nine weld specimens and two base-metal specimens were tested to obtain tensile strength data. A summary of the tensile yield and tensile ultimate strength results is contained in table V. The complete results for each specimen (F_{TU}, F_{TY}, and E) are listed in table VI. The following observations can be made regarding the tensile test results.

1. The tensile properties for the welds had significant scatter, even for duplicate specimens taken from the same welded plate.

2. Except for the pulse GTA welds, all welds subjected to the normal aging temperature and not re-solution treated after welding had approximately the same strength properties as base-metal specimens.

3. For all welds, the yield and ultimate strengths in an LN_2 environment were 10 to 15 percent higher than the room-temperature strengths. (No base-metal results for the LN_2 environment were obtained, but data from reference 2 (listed in table V) show a similar increase in strength.)

4. The re-solution treatment after welding and the exposure to an aging temperature 55.5 K (100° F) higher than normal reduced the room-temperature strength properties of the GTA welds.

Fracture-Toughness Results

The fatigue-crack-growth and fracture data were analyzed using the stress-intensity-factor method. The calculations were made using the following equation for the stress-intensity factor at the minor axis of a semielliptical surface-type flaw.

$$K_a = F\sigma\sqrt{\frac{\pi a}{Q}}\,M \qquad (1)$$

where F is a correction factor for the effect of the cracked plate surface (front face) on the growth of a crack through the thickness, σ is applied stress, M is a correction factor for the effect of crack shape and depth on the growth of a crack through the thickness, and Q is a flaw-shape correction factor given by the equation

$$Q = \Phi^2 - 0.212\left(\frac{\sigma}{F_{TY}}\right)^2 \tag{2}$$

In equation (2), Φ is an elliptic integral of the second kind with the values listed in table VII.

Equation (1) is basically Irwin's expression (ref. 3) for an elliptical crack embedded in an infinite solid, with correction factors F and M applied to account for the finite thickness of the specimens. Correction factor F is for the effect of the free front surface (flawed side) of the plate on growth of the crack through the thickness. It was determined by using the following equation proposed by Kobayashi and Moss (ref. 4).

$$F = 1.0 + 0.12\left(1 - \frac{a}{2b}\right)^2 \tag{3}$$

where b is the crack half-length. The correction factor M is a function of a/t (where t is the plate thickness) and a/2b and accounts for the effect of the back surface on flaw growth through the thickness. The factor was determined by a linear interpolation between Kobayashi's solution for a/2b = 0 and Smith's solution for a/2b = 0.5. The use of the Kobayashi and Smith solutions for backface correction factors is discussed in reference 5. The linear interpolation procedure used for determining M is shown in figure 12. More recent and less approximate solutions exist for the correction factor M, such as that of Kobayashi and Moss (ref. 4). Because it was desired to keep the publication of fracture-toughness values consistent with those of previous programs at JSC, these solutions were not used. Also, because most flaws were not more than approximately halfway through the thickness, the variation in stress-intensity-factor values by using more rigorous solutions for M would not have been significant.

To determine the fracture-toughness values from the test data, equation (1) was written in the following form.

$$K_{IE} = F\sigma_c\sqrt{\frac{\pi a_f}{Q}}\,M \tag{4}$$

where the subscript c indicates conditions at failure and the subscript f indicates final conditions after N cycles. In determining Q for equation (4) (from eq. (2)), the

values of F_{TY} were the average values listed in table V. These calculations were made on each specimen tested, and the fracture-toughness results are listed in tables II to IV and VIII. In table VIII, a summary of the average fracture-toughness results for the base metal and each type of weld and heat treatment is given. In tables II to IV, the detail data for each specimen tested are listed.

In evaluating the results, significant scatter was found in the fracture-toughness values of the welded specimens. Comparing results for the same type weld and heat treatment, the difference between the mean value of K_{IE} and the lowest value of K_{IE} varied between 7 and 22 percent of the mean value for cases in which four or more specimens were tested. The similar variation for base metal was 9 percent at room temperature (15 specimens tested) and 5 percent at LN_2 temperature (4 specimens tested). Some other observations pertaining to the fracture-toughness results are as follows.

1. The average K_{IE} values for weld metal were from 34 to 64 percent of the average K_{IE} value for the base metal at room temperature and 23 to 57 percent of the value at LN_2 temperature.

2. The average K_{IE} values for weld metal were less at LN_2 temperature than at room temperature, whereas the base-metal values were higher at LN_2 temperature than at room temperature.

3. The fracture toughness of the GTA welds was higher than the fracture toughness of either EB or plasma-arc welds.

4. For GTA welds having the same normal aging heat treatment, a re-solution treatment after welding increased the fracture toughness.

5. Exposure after welding to an aging temperature 55.5 K (100° F) higher than normal reduced the fracture toughness.

Fatigue-Crack-Growth Tests

As mentioned previously, the fatigue-crack-growth tests were performed by first applying constant-amplitude stress cycles to develop a fatigue-crack-growth band beyond an initial surface-fatigue crack and then statically loading the specimens to failure. The appearances of the fatigue bands and fracture surfaces for the different types of welds are shown in figure 13. The growth of the fatigue cracks for discrete numbers of fatigue cycles was determined using the crack dimensions a and 2b measured on the distinctive bands. The results are shown in tables II to IV. The experimental crack-growth rate per cycle was then computed, and these results are shown as $(a_f - a_i)/N$ (where the subscript i indicates initial conditions before cycling) in the same tables along with the stress-intensity-factor range for each test.

To determine the stress-intensity-factor range in the fatigue-crack-growth-rate data analysis, equation (1) was put into the following form.

$$\Delta K_a = F\,\Delta\sigma\sqrt{\frac{\pi}{Q}\frac{a_i + a_f}{2}}\,M \tag{5}$$

where

$$Q = \Phi^2 - 0.212\left(\frac{\Delta\sigma}{\frac{1 - R}{F_{TY}}}\right)^2 \tag{6}$$

In equation (6), Irwin's original expression has been modified to account for cyclic loading at different values of R. The values of Φ^2 and F_{TY} used to calculate Q are the same as those used for determining K_{IE} from equation (4).

An examination of the fatigue-crack-growth data plotted in figures 14 to 20 shows no significant differences between the growth rates at room temperature and the growth rates at LN_2 temperature. Other observations with respect to the results are as follows.

1. The crack-growth rate of weld metal was an order of magnitude greater than the growth rate of base metal.

2. The crack-growth rate of the GTA weld metal was not significantly different for the three different heat treatments.

3. The crack-growth rates of EB and PAW-GTA welded specimens were approximately the same. Both of these rates were greater than the growth rate of GTA welded specimens.

Correlation of Crack-Growth Data With Analysis

Because fatigue-crack-growth rate is a complicated function of the stress-intensity-factor range ΔK plus other secondary effects, to evaluate test results directly is not easy. The most pertinent results are obtained by first correlating the test data with a satisfactory fatigue-crack-growth-rate equation. This procedure not only provides an analytical model for comparing fatigue-crack-growth-rate results but also gives information on the ability to calculate fatigue-crack-growth behavior accurately. This ability is imperative for developing an adequate fracture control plan for reusable pressure vessels or for structures with possible preexisting flaws.

Using the same approach used in reference 1, the fatigue-crack-growth-rate equation obtained from reference 6 was selected to correlate with the experimental data. This equation was found to correlate satisfactorily with 2219-T87 aluminum weld and

base-metal data, for growth in the crack depth direction as reported in references 1 and 7. For the analysis of semielliptical surface-type flaws, the equation is expressed as follows.

$$\frac{da}{dN} = \frac{C_a(\Delta K_a)^S}{(1 - R)K_{IE} - \Delta K_a} \tag{7}$$

To determine the empirical constants C_a and S, equation (7) is rewritten as follows.

$$\left[(1 - R)K_{IE} - \Delta K_a\right]\frac{da}{dN} = C_a(\Delta K_a)^S \tag{8}$$

Equation (8) plots as a straight line on log-log coordinates and is referred to as the linearized form of equation (7). All crack-growth-rate test data from tables II to IV were plotted in this linearized form, and the results are shown in figures 21 to 24. A straight line was then drawn through the data points to derive the constants C_a and S. The reasonably good agreement between the straight line and the data points confirms the validity of equation (7).

Values of the empirical constants C_a and S that produced the most accurate curve fits are listed in table IX. The values of K_{IE} used in calculating the data points in figures 21 to 24 were the specific values listed for each specimen. These values were used because the correlation when using the average K_{IE} values (listed in table VIII) was not as good. Also, many points (at higher ΔK values) could not have been plotted. This inability occurred when $\Delta K(1 - R)$ exceeded average K_{IE} for which the abscissa $(1 - R)K_{IE} - \Delta K \leq 0$.

The good agreement when using the same value of $S = 3.7$ for both base metal and all types of weld metal is worth additional comparisons because this agreement did not occur in the reference 1 studies on thick aluminum welds. To further evaluate the empirical constants in equation (8), some additional 0.28-centimeter (0.11 inch) thick Inconel 718 plate data from reference 8 were plotted in the linearized form. The results are shown in figures 25 and 26 for weld and base metal, respectively. The thin-plate data show good agreement with equation (8), and the value of $S = 3.7$ is the same as that obtained in the thick-plate results. No change is observed for the value of C_a for weld metal, but it increased approximately 50 percent for base metal.

To evaluate the accuracy of equation (7) when average values of K_{IE} are used, a correlation between experimental and theoretical crack-growth rates for a load ratio of 0.05 is shown in figures 14 to 20. Also, to determine the accuracy for a different load ratio R, a correlation is shown in figure 27 for an R value of 0.5. Essentially,

these correlations with experimental data, such as in figures 21 to 24, show that a scatter factor of 4 would be required in crack-growth-rate predictions for Inconel 718, the same as earlier found for 2219 aluminum.

Another important correlation is that between the theoretical and experimental crack-growth rate on the surface of the specimens. The theoretical growth rate is predicted by the following equation, which is essentially the same as equation (7) for growth through the thickness.

$$\frac{db}{dN} = \frac{C_b(\Delta K_b)^S}{(1 - R)K_{IE} - \Delta K_b} \tag{9}$$

In equation (9), ΔK_b is the stress-intensity factor at the point where the crack tip meets the specimen surface and C_b is the empirical constant for growth rate at that point. The simultaneous use of equations (7) and (9) and the appropriate solutions for ΔK_a and ΔK_b are discussed in reference 7. The expression for ΔK_b can be written as follows.

$$\Delta K_b = 1.12\ \Delta\sigma\left(\frac{a}{b}\right)\sqrt{\frac{\pi L}{Q}} \tag{10}$$

where $a = (a_i + a_f)/2$ and $b = (b_i + b_f)/2$. With the use of equation (10), the stress-intensity-factor ranges were calculated for the base-metal-specimen results and the values plotted against the measured db/dN in figure 28. A best fit for equation (9) is also compared with the experimental results.

Except for two points, the comparison between theoretical and experimental results is very good. The comparison also shows that the constant C_b has approximately twice the value of C_a. This same relationship between C_a and C_b was reported previously for 2219 aluminum data in reference 7. A comparison of C_a with C_b was not attempted for weld metal in either Inconel 718 or 2219 aluminum because of the excessive scatter in the data.

Application of the proper relationship between growth of a crack at the specimen surface and growth through the thickness has a significant effect on calculating fatigue life. For instance, using equations (7) and (9), the predicted number of cycles to fracture would be less when assuming $C_b = 2C_a$ than when assuming $C_b = C_a$. Other factors also affect the relationship between growth on the surface and growth through the thickness, and these factors will be discussed in more detail.

One reason for the variation in crack-growth rate along the crack front of a surface flaw is that the elastic constraint at the crack tip varies around the crack perimeter. The crack-tip material at the specimen surface is usually considered to be in a state of plane stress, whereas the material at the maximum crack depth is considered to be in a state of plane strain. The difference in constraint not only affects the values of C_a and C_b but also the magnitude of the stress-intensity-factor ranges ΔK_a and ΔK_b given by equations (5) and (10), respectively. The factor Q given by equation (6) enters into both of these equations and was derived by assuming a plane-strain yield-zone radius at the crack tip. Essentially, the derivation of Q assumed an effective crack depth of $a + r_y$ where r_y is the yield-zone radius given by the equation

$$r_y = \frac{1}{(4\sqrt{2})\pi}\left(\frac{K}{F_{TY}}\right)^2 \tag{11}$$

and the resulting equation for Q can be applied both at the specimen surface and at the maximum crack depth. For the specimen surface, however, a more precise derivation of effective crack length is to let the length equal $b + r_x$ where r_x is the well-known plane-stress yield-zone radius given by the equation

$$r_x = \frac{1}{2\pi}\left(\frac{K}{F_{TY}}\right)^2 \tag{12}$$

By comparing equations (11) and (12), it can be seen that r_x is 2.83 times larger than r_y. This difference has been observed experimentally in surface-crack yield-zone measurements and is reported in reference 9. A similar approach to the problem by assuming the two different stress states has been proposed in reference 10.

By making the plane-stress modification to Irwin's solution, a different equation for ΔK_b can then be rewritten as

$$\Delta K_b = \frac{1.12}{\Phi}\,\Delta\sigma\left(\frac{a}{b}\right)\sqrt{\pi\left(b + r_x\right)} \tag{13}$$

Substituting equation (12) into equation (13), letting $K = \Delta K_b/(1 - R)$, and solving for ΔK_b gives the plane-stress corrected solution

$$\Delta K_b = 1.12\,\Delta\sigma\left(\frac{a}{b}\right)\sqrt{\frac{\pi b}{Q_b}} \tag{14}$$

where

$$Q_b = \Phi^2 - 0.627\left(\frac{a}{b}\right)^2\left(\frac{\Delta\sigma}{\frac{1-R}{F_{TY}}}\right)^2 \qquad (15)$$

The preceding equations indicate that the plane-stress yield-zone assumption changes the value of ΔK_b and, thus, affects the fatigue-crack-growth rate. The difference in the calculated values of ΔK_b between use of equations (6) and (15) for the factor Q is not significant, however, when a/2b is equal to approximately 0.3. Fortunately, the Inconel 718 results in this report and the 2219 aluminum results in reference 7 are for values of a/2b equal to approximately 0.3. The conclusion can be made that letting $C_b = 2C_a$ is adequate because the improved solution for ΔK_b did not affect the correlation with the test results. This conclusion may not be true for either semicircular or long shallow cracks, however, and to understand this difficulty would require additional investigation.

CONCLUSIONS

The results of the test program to investigate fracture toughness and crack-growth behavior in thick welded plates of Inconel 718 can be summarized as follows.

1. The welding of 1.90-centimeter (0.75 inch) thick Inconel 718 is feasible. The gas tungsten arc process resulted in the least difficulties and the highest fracture-toughness properties.

2. For gas tungsten arc welds having the same normal aging heat treatment, a re-solution treatment after welding gave an increase in fracture toughness but did not significantly affect the tensile ultimate strength or the crack-growth rate.

3. Exposure to an aging temperature 55.5 K (100° F) higher than normal reduced the fracture-toughness value but did not significantly affect the tensile ultimate strength or the crack-growth rate.

4. The fatigue-crack-growth rate for weld metal was an order of magnitude greater than the growth rate for base metal.

5. The crack-growth rates of electron-beam-welded specimens and specimens that were plasma-arc root welded with gas tungsten arc fill passes were approximately the same. Both these rates were greater than the growth rate of gas tungsten arc welded specimens.

6. The fatigue-crack-growth-rate experimental data correlated satisfactorily with analytical results.

Lyndon B. Johnson Space Center
National Aeronautics and Space Administration
Houston, Texas, February 14, 1974
968-15-11-01-72

REFERENCES

1. Forman, Royce G.; Glorioso, Samuel V.; and Medlock, James D.: Flaw Growth Behavior in Thick Welded Plates of 2219-T87 Aluminum at Room and Cryogenic Temperatures. NASA TN D-7377, 1973.

2. Anon.: Aerospace Structural Metals Handbook. Vol. III, AFML-TR-68-115, Air Force Materials Laboratory, Air Force Systems Command, Wright-Patterson Air Force Base, Ohio, 1971.

3. Irwin, G. R.: The Crack Extension Force for a Part-Through Crack in a Plate. Trans. ASME, Ser. E, J. Appl. Mech., vol. 29, no. 4, Dec. 1962, pp. 651-654.

4. Kobayashi, A. S.; and Moss, W. L.: Stress Intensity Magnification Factors for Surface-Flawed Tension Plate and Notched Round Tension Bar. Paper presented at the Second International Conference on Fracture (Brighton, England), Apr. 13-18, 1969.

5. Tiffany, C. F.: Fracture Control of Metallic Pressure Vessels. NASA SP-8040, 1970.

6. Forman, R. G.; Kearney, V. E.; and Engle, R. M.: Numerical Analysis of Crack Propagation in Cyclic-Loaded Structures. Trans. ASME, Ser. D, J. Basic Eng., vol. 89, no. 3, Sept. 1967, pp. 459-464.

7. Forman, Royce G.; Kavanaugh, Herbert C.; and Stuckey, Bernard: Computer Analysis of Two-Dimensional Fatigue Flaw-Growth Problems. NASA TM X-58086, 1972.

8. Pettit, D. E.; Feddersen, C. E.; and Mindlin, H.: Flaw Growth Behavior of Inconel 718 at Room and Cryogenic Temperature. NASA CR-101942, 1969.

9. Francis, Philip H.; Davidson, David L.; and Forman, Royce G.: An Experimental Investigation into the Mechanics of Deep Semielliptical Surface Cracks in Mode I Loading. Eng. Fracture Mech., vol. 4, 1972, pp. 617-635.

10. Francis, P. H.: On the Configuration of a Propagating Surface Fatigue Crack. Appl. Sci. Res., vol. 25, no. 1-2, Nov. 1971, pp. 26-34.

TABLE I.- CHEMICAL ANALYSIS OF

NASA-PURCHASED INCONEL 718[a]

Element	Content, percent
Cobalt	0.34
Iron	19.10
Boron	.005
Carbon	.05
Sulfur	.006
Phosphorus	.003
Silicon	.06
Manganese	.1[illegible]
Molybdenum	3.14
Copper	.01
Chromium	18.00
Aluminum	.52
Titanium	1.01
Columbium	5.02
Nickel	Balance

[a]Used for Phase II specimens; purchased from Cabot Corporation, Stellite Division (heat no. 2180-0-9195), to specification AMS-5596 INCO 718.

TABLE II.- CRACK-GROWTH TEST RESULTS FOR GTA AND PULSE GTA WELDED INCONEL 718 SPECIMENS

(a) SI units

Specimen number	Test environment	t, cm	w, cm	$\Delta\sigma$, MN m^2	R	N, cycles	Cyclic frequency, Hz	σ_c, MN/m^2	a_i, cm	$2b_i$, cm	a_f, cm	$2b_f$, cm	$\frac{a_f - a_i}{N}$, nm/cycle	$\Delta K_{avg.}$, $MN/m^{3/2}$	K_{IE}, $MN/m^{3/2}$
GTXA-1	RT[a] air	1.88	9.712	--	--	0	--	436	--	--	0.698	2.29	--	--	58.2
GTXA-2	LN_2	1 71	9.354	--	--	0	--	472	--	--	.698	2.13	--	--	61.7
GTXA-3	LN_2	.80	9.416	--	--	0	--	553	--	--	.597	2.03	--	--	68.9
GTXA-4	RT air	1.88	9.644	--	--	0	--	599	--	--	.559	1.79	--	--	70.7
GTXA-5	RT air	1.87	9.792	--	--	0	--	691	--	--	.724	2.11	--	--	91.2
GTNA-11	RT air	1.26	7 630	263	0.05	5 000	2	572	0.586	1.78	.780	2.01	381	33.4	77.4
GTNA-13	RT air	1.33	7.643	350	.05	1 500	1	648	.653	2.04	.813	2.35	1 067	48.0	95.8
GTNA-14	RT air	1.37	7.640	170	.05	15 000	2	722	.584	2.07	.673	2.13	51	21.8	97.5
GTNA-15	RT air	1.33	7.633	415	05	200	.5	[illegible]	.622	1.9[illegible]	.658	2.02	1 780	53.3	107.5
GTNA-16	RT air	1.51	7 640	439	.05	50	5	[illegible]	.650	1.86	.668	1.88	3 560	54.4	84.0
GTNA-17	RT air	1.28	7.643	562	.05	100	.5	[illegible]	640	1.95	.767	2.00	[illegible]	73 8	87.8
GTNA-18	LN_2	1.34	7.640	247	05	5 000	2	7[illegible]	610	1.87	673	1 95	1[illegible]7	30.9	95 0
GTNA-19	LN_2	1.41	7.635	330	.05	1 500	1	5[illegible]	. 83	1.88	.851	1.99	1 120	42 4	70.5
GTNA-110	LN_2	1.44	7.643	384	05	400	.5	550	.676	1.93	.856	2 00	4 520	49.7	73.0
GTNA-111	LN_2	1.49	7.638	483	.05	100	.5	807	.653	1.82	.678	1.84	2 540	59.3	101 4
GTNA-31	LN_2	1.49	7.628	559	.05	39	.5	[b]589	.493	(c)	.546	1.91	13 700	66 8	71 4
GTNA-34	LN_2	1.62	7.635	511	.05	50	.5	592	.589	2.10	.739	2.37	30 000	67.8	82.5
GTNA-35	RT air	1.47	7.625	564	.05	50	.5	673	.495	1.81	.551	1.86	11 200	66 9	81.9
GTNA-36	RT air	1.40	7.628	473	.05	150	.5	664	.510	1.85	.546	1.93	2 360	56.8	81.9
GTNA-37	RT air	1.46	7.633	204	.05	11 277	.5	717	.528	1.78	.610	1.95	76	24.5	91.0
GTNB-24	RT air	1.66	7.633	267	.05	5 000	2	667	.561	1.87	.650	1.89	180	32.3	83.8
GTNB-25	RT air	1.67	7.635	365	.05	1 000	1	804	.526	1.86	.62[illegible]	1.93	940	44 0	102.2
GTNB-26	LN_2	1.68	7.635	263	.05	5 000	2	676	.602	1.76	.640	1.81	76	31 3	82.4
GTNB-27	RT air	1.66	7.633	166	.05	15 000	2	945	.587	1.81	.630	1.85	25	19 8	120.0
GTNB-28	LN_2	1.67	7.64[illegible]	365	.05	1 000	1	914	.525	1.75	.551	1.77	254	42.2	100.0
GTNB-29	RT air	1.63	7.632	543	.05	100	.5	978	.477	1.77	.523	1.80	4 570	62.9	109.5
GTNB-210	LN_2	1.67	7.640	531	.05	100	.5	786	.493	1.83	.554	1.85	6 100	62.3	86 6
GTNB-211	RT air	1 61	7.635	411	.05	200	.5	675	.612	1.82	.685	1.86	3 680	50 2	77.2
GTNC-22	RT air	1.70	7.638	261	.05	5 000	2	607	.526	1.90	.640	2.07	229	31.9	71.2
GTNC-23	RT air	1.70	7.638	360	.05	1 000	1	781	.480	1.74	.536	1.80	559	41.2	85.4
GTNC-32	LN_2	1.50	7.635	258	.05	5 000	2	643	.470	1.73	.508	1.77	76	29.2	68.2
GTNC-38	RT air	1.51	7.628	161	.05	15 000	2	636	546	1.77	.577	1.79	25	18 8	69.9
GTNC-39	LN_2	1.55	7.640	393	.05	1 000	1	466	.559	1.86	.942	2.03	3 830	50.1	56.1
GTNC-310	RT air	1.43	7.630	542	.05	100	.5	603	.538	1.81	.625	1.92	8 640	66.4	69.4
GTYA-2	RT air	1.62	7.630	273	.05	5 000	2	614	.493	1.77	.699	2.13	406	33.4	74.3
GTYA-3	RT air	1.68	7.630	363	.05	1 000	1	776	.513	1.79	.589	1.93	760	43.1	88.6
GTYA-4	LN_2	1.70	7.628	261	.05	5 000	2	508	.541	1.80	.706	2.01	330	31.8	59.2
GTYA-6	LN_2	1.78	7.643	341	.05	1 000	1	728	.513	1.77	.541	1.84	280	39.5	79.0
GTYA-7	RT air	1.73	7.645	510	.05	38	.5	[b]537	.508	1.76	.523	1.79	4 010	59.0	57.1
GTYA-9	LN_2	1.69	7.648	425	.05	200	.5	715	.521	1.78	.543	1.86	1 140	49.6	78.2
GTYA-10	RT air	1.63	7.635	441	.05	200	.5	553	.571	1.90	.716	2.09	7 240	55.6	66.4

[a]RT = room temperature

[b]Specimen failed during fatigue loading

[c]Difficult to distinguish between initial and final flaw size.

TABLE II. - CRACK-GROWTH TEST RESULTS FOR GTA AND PULSE GTA WELDED INCONEL 716 SPECIMENS - Concluded

(b) U.S. customary units

Specimen number	Test environment	t, in.	w, in.	$\Delta\sigma$, ksi	R	N, cycles	Cyclic frequency, cps	σ_c, ksi	a_i, in.	$2b_i$, in	a_f, in.	$2b_f$, in	$\frac{a_f - a_i}{N}$, μin/cycle	$\Delta K_{avg.}$, ksi $\sqrt{in}$	K_{IE}, ksi $\sqrt{in.}$
GTXA-1	RT[a] air	0.740	3.824	--	--	0	--	63.3	--	--	0.275	0.900	--	--	53.0
GTXA-2	LN_2	.675	3.683	--	--	0	--	68.4	--	--	.275	.840	--	--	56.1
GTXA-3	LN_2	.710	3.707	--	--	0	--	80.2	--	--	.235	.800	--	-	62.7
GTXA-4	RT air	.739	3.797	--	--	0	--	86.9	--	--	.220	.705	--		64.4
GTXA-5	RT air	.735	3.755	--	--	0	--	100.2	--	--	.265	.850	--	-	83.0
GTNA-11	RT air	.498	3.004	38.1	.5	5 000	2	82.9	0.231	0.700	.307	.790	15	30.4	70 5
GTNA-13	RT air	.523	3.009	50.7	.05	1 500	1	94.0	.257	.803	.320	.925	42	43.7	87.2
GTNA-14	RT air	.539	3.008	24.6	.05	15 000	2	104.8	.230	.814	.265	.837	2	19.9	88.8
GTNA-15	RT air	.525	3.005	60.2	.05	200	.5	117.3	.245	.784	.259	.797	70	48.5	97.9
GTNA-16	RT air	.595	3.008	63.7	.05	50	.5	96.7	.256	.732	.263	.741	140	49.5	76.4
GTNA-17	RT air	.505	3.009	81.5	.05	100	.5	94.1	.252	.766	.302	.788	500	67 2	79.8
GTNA-18	LN_2	.528	3.008	35.9	.05	5 000	2	106.3	.240	.738	.265	.766	5	28.1	86.5
GTNA-19	LN_2	.555	3.006	47.8	.05	1 500	1	77 1	.2[illegible]	.740	.335	.783	44	38.6	64.2
GTNA-110	LN_2	.567	3.009	55.7	.05	400	.5	.7	.266	.760	.337	.788	178	45.2	66.4
GTNA-111	LN_2	.587	3.007	70.0	.05	100	.5	117.0	.257	.718	.267	.726	100	54 0	92.3
GTNA-31	LN_2	.535	3.003	81.1	.05	39	.5	[b]65 4	.194	(c)	.215	.751	538	60.8	65.0
GTNA-34	LN_2	.639	3.006	74.2	.05	50	.5	85.9	.232	.829	.291	.932	1180	61.7	75.0
GTNA-35	RT air	.580	3.002	81.8	.05	50	.5	97.6	.195	.712	.217	.733	440	60.9	74.5
GTNA-36	RT air	.553	3.003	68.6	.05	150	.5	96.3	.201	.730	.215	.760	93	51.7	74.6
GTNA-37	RT air	.576	3.005	29.6	.05	11 277	.5	104.0	.208	.702	.240	.770	3	22.3	82.8
GTNB-24	RT air	.653	3.005	38.7	.05	5 000	2	96.8	.221	.735	.256	.746	7	29.4	76.2
GTNB-25	RT air	.656	3.006	53.0	.05	1 000	1	116.6	.207	.733	.244	.760	37	40.1	93 '
GTNB-26	LN_2	.661	3.006	36 2	.05	5 000	2	98.1	.237	.694	.252	.713	3	28.5	75.0
GTNB-27	RT air	.655	3.005	24.1	.05	15 000	2	137.1	.231	.713	.248	.727	1	18.1	109.2
GTNB-28	LN_2	.657	3.008	52.9	.05	1 000	1	132.6	.207	.688	.217	.697	10	38.4	100.0
GTNB-29	RT air	.643	3.005	78.7	.05	100	.5	141.8	.188	.698	.206	.710	180	57.3	109.5
GTNB-210	LN_2	.656	3.008	77.0	.05	100	.5	114.0	.194	.720	.218	.728	240	56.7	86.6
GTNB-211	RT air	.636	3.006	59.6	.05	200	.5	97.9	.241	.717	.270	.733	145	45.6	77.2
GTNC-22	RT air	.667	3.007	37.8	.05	5 000	2	88.0	.207	.749	.252	.815	9	[illegible]0.0	71.2
GTNC-23	RT air	.666	3.007	52.2	.05	1 000	1	113.3	.189	.685	.211	.708	22	37.5	85.4
GTNC-32	LN_2	.592	3.006	37.4	.05	5 000	2	93.3	.185	.681	.200	.695	3	26.6	68.2
GTNC-38	RT air	.596	3.003	23.3	.05	15 000	2	92.2	.215	.698	227	.706	1	17.1	69.9
GTNC-39	LN_2	.610	3.008	57.0	.05	1 000	1	67.6	.220	.732	.371	798	151	45.5	56.1
GTNC-310	RT air	.563	3.004	78.6	.05	100	.5	87.5	.212	.713	.246	.758	340	60.4	69.4
GTYA-2	RT air	.639	3.004	39.6	.05	5 000	2	89.1	.194	.698	.21[illegible]	.837	16	[illegible]0.4	74.3
GTYA-3	RT air	.660	3.004	52.7	.05	1 000	1	112.5	.202	.704	.232	.759	30	39 [illegible]	88.6
GTYA-4	LN_2	.669	3.003	37.8	.05	5 000	2	73.7	.213	.709	.278	.790	13	28.	59.2
GTYA-6	LN_2	.702	3.009	49.5	.05	1 000	1	105.6	.202	.697	.213	722	11	35.[illegible]	79.0
GTYA-7	RT air	.682	3.010	74.0	.05	39	.5	[b]77.9	.200	.692	.206	.704	158	53.[illegible]	67.1
GTYA-9	LN_2	.686	3.011	61.6	.05	200	.5	103.7	.205	.700	.214	.733	45	45.2	78.2
GTYA-10	RT air	.643	3.006	63.9	.05	200	.5	80.2	.225	.749	.282	.825	285	50.6	66.4

[a]RT - room temperature.

[b]Specimen failed during fatigue loading.

[c]Difficult to distinguish between initial and final flaw size.

TABLE III. - CRACK-GROWTH TEST RESULTS FOR EB AND PAW-GTA WELDED INCONEL 718 SPECIMENS

(a) SI units

Specimen number	Test environment	t, cm	w, cm	$\Delta\sigma$, MN/m^2	R	N, cycles	Cyclic frequency, Hz	σ_c, $MN\ m^2$	a_i, cm	$2b_i$, cm	a_f, cm	$2b_f$, cm	$\frac{a_i - a_i}{N}$, nm/cycle	$\Delta K_{avg.}$, $MN/m^{3/2}$	K_{IE}, $MN/m^{3/2}$
EBXA-1	RT[a] air	1.68	8.880	283	0.05	334	2	[b]298	0.795	2.04	1.24	2.72	13 500	40.7	46.8
EBXA-2	RT air	1.69	8.877	--	--	0	--	341	--	--	.792	2.08	--	--	44.8
EBXA-3	LN_2	1.77	8.885	--	--	0	--	333	--	--	.836	2 02	--	--	43.0
EBXA-4	LN_2	1.58	8.882	181	.05	4 000	2	254	785	1 91	.922	2.11	330	23 5	34.2
EBXA-5	RT air	1.75	10.17	143	.05	30 000	2	476	.642	1.85	.856	1.93	76	17.7	60 6
EBXA-6	RT air	1.91	10.16	218	.05	5 000	1	492	.643	1.81	.818	1.88	356	26 5	61.5
EBNA-2	RT air	1.65	8.339	123	.05	17 000	2	501	.795	1.92	.904	2.08	64	15.9	67.0
EBNA-3	RT air	1.75	8.351	231	.05	3 885	1	609	.770	1.91	.914	2.06	381	29.6	80.8
EBNA-4	LN_2	1.64	8.227	125	.05	15 000	2	445	.742	1.86	.797	1.93	36	15.7	56.5
EBNA-5	LN_2	1.75	8.230	235	.05	3 000	1	458	.757	2.00	.924	2.07	559	30.6	60.6
EBNA-6	RT air	1.69	8.169	366	.05	575	.5	498	.676	1.83	1.09	2.32	7 160	48.5	71.0
EBNA-7	RT air	1.76	8.171	294	.05	784	.5	611	.701	1.79	.825	1.85	1 570	35.9	76.3
EBNA-8	RT air	1.78	8.174	407	.05	70	.5	576	.693	1.85	.737	1.89	6 170	50.2	72 2
EBNA-9	LN_2	1.73	8.184	298	.05	500	5	502	.770	1.94	.864	1.99	1 880	38.0	64.5
PAXA-1	RT air	1.84	10.05	183	.05	9 000	2	401	683	1.79	.823	2.19	150	23.2	54.0
PAXA-2	RT air	1.91	10.17	260	.05	2 000	1	439	.549	1.86	.729	2.22	890	32.4	58.3
PAXA-3	LN_2	1.87	10.17	178	.05	9 000	2	386	.612	1.88	.719	2.18	130	22.3	50.7
PAXA-4	RT air	1.83	10.16	136	.05	16 500	2	509	.577	1.82	.635	1.90	25	16.3	62.5
PAXA-5	LN_2	1.86	10.17	267	05	1 000	1	453	.572	1.82	.630	1.87	584	31.8	54.8
PAXA-6	RT air	1.94	10.18	214	.05	2 270	1	490	.546	1.82	.637	1.94	406	25.5	60.5

[a]RT = room temperature.

[b]Specimen failed during fatigue loading.

(b) U.S. customary units

Specimen number	Test environment	t, in.	w, in.	$\Delta\sigma$, ksi	R	N, cycles	Cyclic frequency, cps	σ_c, ksi	a_i, in.	$2b_i$, in.	a_f, in.	$2b_f$, in.	$\frac{a_f - a_i}{N}$, μin/cycle	$\Delta K_{avg.}$, $ksi\sqrt{in.}$	K_{IE}, $ksi\sqrt{in.}$
EBXA-1	RT[a] air	0.6625	3.495	41.0	0.05	334	2	[b]43.2	0.313	0.803	0.490	1.070	530	37.1	42.6
EBXA-2	RT air	.6655	3.495	--	--	0	--	49.4	--	--	.312	.819	--	--	40.7
EBXA-3	LN_2	.6985	3.498	--	--	0	--	48.3	--	--	.329	.794	--	--	39.2
EBXA-4	LN_2	.6210	3.497	26.2	.05	4 000	2	36.8	.309	.751	.363	.833	13	21.4	31.1
EBXA-5	RT air	.688	4.004	20.7	.05	30 000	2	69.0	.253	.728	.337	.762	3	16.1	55.2
EBXA-6	RT air	.752	4.002	31.6	05	5 000	1	71.4	.253	.709	.322	742	14	24.1	55.9
EBNA-2	RT air	.649	3.283	17.8	05	17 000	2	72.7	.313	.756	.356	.818	2.5	14.4	61.0
EBNA-3	RT air	.689	3.288	33.5	.05	3 885	1	88.3	.303	.750	.360	.810	15	26.9	73.6
EBNA-4	LN_2	.646	3.239	18.2	.05	15 000	2	64.5	.292	.734	.314	.760	1.4	14.3	51 4
EBNA-5	LN_2	.688	3.240	34.1	.05	3 000	1	66.4	.298	.788	.364	.817	22	27.8	55.1
EBNA-6	RT air	.667	3.216	53.1	.05	575	.5	72.3	.266	.722	.428	.913	282	44.1	64.6
EBNA-7	RT air	.692	3.217	42.7	.05	784	.5	88.7	.276	.704	.325	.727	62	32.7	69.4
EBNA-8	RT air	700	3.218	59.0	.05	70	.5	83.5	.273	.727	.290	.745	243	45.7	65.7
EBNA-9	LN_2	.682	3.222	43.2	.05	500	.5	72.8	.303	.766	.340	.783	74	34.6	59.0
PAXA-1	RT air	.725	3.956	26.5	.05	9 000	2	58.2	.269	.706	.324	.863	6	21.1	49.1
PAXA-2	RT air	.754	4.005	37.7	.05	2 000	1	63.6	.216	.731	.287	.875	35	29.5	53.0
PAXA-3	LN_2	.735	4.005	25.°	.05	9 000	2	56.0	.241	.742	.283	.860	5	20.3	46.1
PAXA-4	RT air	.720	4.001	19.8	.05	16 500	2	73.8	.227	.718	.250	.747	1	14.8	56.9
PAXA-5	LN_2	.733	4.005	38.8	.05	1 000	1	65.7	.225	.718	.248	.735	23	29.0	49.9
PAXA-6	RT air	.764	4.006	31.0	.05	2 270	1	71.1	.215	.715	.251	.763	16	23.2	55.0

[a]RT = room temperature.

[b]Specimen failed during fatigue loading.

TABLE IV.- CRACK-GROWTH TEST RESULTS FOR INCONEL 718 BASE-METAL SPECIMENS

(a) SI units

Specimen number	Test environment	t, cm	w, cm	$\Delta\sigma$, MN/m^2	R	N, cycles	Cyclic frequency, Hz	σ_c, MN/m^2	a_i, cm	$2b_i$, cm	a_f, cm	$2b_f$, cm	$\frac{a_f - a_i}{N}$, nm/cycle	$\Delta K_{avg.}$, $MN/m^{3/2}$	K_{IE}, $MN/m^{3/2}$
BANA-1	RT[a] air	1.86	8.562	265	0.05	10 000	2	1210	0.488	1.796	0.493	1.796	5	30.0	148.6
BANA-2	RT air	1.85	8.560	444	.01	10 000	2	1260	.508	1.819	.826	2.103	318	55.4	176.6
BANA-3	RT air	1.85	8.517	536	.05	4 500	1	1300	.472	1.780	.711	1.986	533	64.8	175.5
BANA-4	RT air	1.85	8.537	802	.05	318	1	1340	.541	1.760	.594	1.811	1 676	95.7	171.8
BANA-11	RT air	1.87	8.009	452	.05	5 000	1	1300	.356	1.758	.394	1.783	76	47.8	153.2
BANA-12	RT air	1.89	8.412	318	.05	20 000	1	1310	.381	1.786	.409	1.793	13	33.8	152.3
BANA-13	RT air	1.88	8.679	986	.05	666	.5	1280	.330	1.770	.508	1.890	2 670	113.1	162.4
BANA-14	RT air	1.86	8.738	1040	.05	203	.5	1280	.378	1.783	.409	1.795	1 500	117.3	152
BANA-15	RT air	1.84	8.694	900	.05	300	.5	1320	.307	1.763	.350	1.780	1 450	94.7	152.7
BANA-16	LN_2	1.86	8.687	887	.05	400	.5	1390	.434	1.773	.478	1.798	1 070	101.4	169.5
BANA-17	LN_2	1.89	9.101	980	.05	150	.5	1390	.424	1.808	.467	1.834	2 870	112.8	156.4
BANA-18	RT air	1.88	8.946	--	--	0	--	1300	--	--	.363	1.775	--	--	150.9
BANA-19	RT air	1.89	8.860	1010	.05	100	.5	1290	.429	1.798	.475	1.834	4 570	117.8	159.8
BANA-20	RT air	1.88	8.943	527	.50	2 000	.5	1220	.401	1.780	.650	2.024	1 240	61.8	162.5
BANA-21	RT air	1.91	9.014	1130	.05	40	.5	1260	.495	1.760	.556	1.801	15 200	136.7	158.5
BANA-24	RT air	1.86	9.528	810	.05	500	.5	1130	.810	2.050	1.003	2.311	3 860	111.3	165.3
BANA-25	LN_2	1.89	9.746	778	.05	500	.5	1340	.454	2.009	.503	2.042	965	92.5	171.3
BANA-26	RT air	1.89	9.568	368	.50	3 001	1	1120	.564	2.050	.729	2.230	560	46.8	157.4
BANA-27	LN_2	1.88	9.563	517	.05	2 000	1	1230	.823	1.986	.935	2.131	560	67.8	173.5

[a]RT = room temperature.

(b) U.S. customary units

Specimen number	Test environment	t, in	w, in.	$\Delta\sigma$, ksi	R	N, cycles	Cyclic frequency, cps	σ_c, ksi	a_i, in.	$2b_i$, in.	a_f, in.	$2b_f$, in.	$\frac{a_f - a_i}{N}$, μin/cycle	$\Delta K_{avg.}$, $ksi\sqrt{in.}$	K_{IE}, $ksi\sqrt{in.}$
BANA-1	RT[a] air	0.734	3 371	38.4	0.05	10 000	2	176	0 192	0.707	0 194	0.707	0.2	27.3	135.2
BANA-2	RT air	.730	3.370	64.4	.01	10 000	2	183	.200	.716	.325	.828	12.5	50.4	160.7
BANA-3	RT air	.728	3.353	77.8	.05	4 500	1	188	.186	.701	.280	.782	21	59.0	159.7
BANA-4	RT air	.729	3.361	116.3	.05	318	1	194	.213	.693	.234	.713	66	87.1	156.3
BANA-11	RT air	.736	3.153	65.5	.05	5 000	1	188	.140	.692	.155	.702	3	43.5	139.4
BANA-12	RT air	.745	3.312	46.2	.05	20 000	1	190	.150	.703	.161	.706	.5	30.8	138.6
BANA-13	RT air	.741	3.417	143.0	.05	666	.5	186	.130	.697	.200	.744	105	103.0	147.8
BANA-14	RT air	.733	3.440	150.7	.05	203	.5	186	.149	.702	.161	.707	59	106.8	139.1
BANA-15	RT air	.723	3.423	130.5	.05	300	.5	192	.121	.694	.138	.701	57	86.2	138.9
BANA-16	LN_2	.734	3.420	128.7	05	400	.5	201	.171	.698	.188	.708	42	92.3	154.2
BANA-17	LN_2	.746	3.583	142.2	.05	150	.5	202	.167	.712	.184	.722	113	102.7	142.4
BANA-18	RT air	.742	3.522	--	--	0	--	189	--	--	.143	.699	--	--	137.3
BANA-19	RT air	.745	3.488	146.2	.05	100	.5	187	.169	.708	.187	.722	180	107.2	145.4
BANA-20	RT air	.742	3.521	76.5	.50	2 000	.5	177	.158	.701	.256	.797	49	56.2	148.8
BANA-21	RT air	.752	3.549	163.7	.05	40	.5	183	.195	.693	.219	.709	600	124.4	144.2
BANA-24	RT air	.733	3.751	117.5	.05	500	.5	164	.319	.807	.395	.910	152	101.3	150.4
BANA-25	LN_2	.746	3.837	112.8	.05	500	.5	194	.179	.791	.198	.804	38	84.2	155.9
BANA-26	RT air	.745	3.767	53.4	.50	3 001	1	163	.222	.807	.287	.878	22	42.6	143.2
BANA-27	LN_2	.740	3.765	75.0	.05	2 000	1	179	.324	.782	.368	.839	22	61.7	157.9

[a]RT = room temperature.

TABLE V. - SUMMARY OF AVERAGE TEST RESULTS FOR F_{TY} AND F_{TU}

Specimen number prefix	Type of weld or metal	No. of specimens	Welding contractor	Base-metal supplier	Postweld heat treatment (a)	F_{TY} average				F_{TU} average			
						Ambient air		LN_2		Ambient air		LN_2	
						MN/m^2	ksi	MN/m^2	ksi	MN/m^2	ksi	MN/m^2	ksi
GXA	GTA	2	X	Contractor X	A[b]	1158	168	--	--	1351	196	--	--
GNA	GTA	5	X	NASA	A	1117	162	1234	179	1365	198	1517	220
GNB	GTA	3	X	NASA	B	1027	149	1220	177	1289	187	1531	222
GNC	GTA	3	X	NASA	C	1041	151	1227	178	1289	187	1531	222
GYA	GTA	4	Y	NASA	A	1041	151	1207	175	1220	177	1565	227
EXA	EB	6	X	Contractor X	A	1103	160	1330	193	1379	200	1544	224
ENA	EB	2	X	NASA	A	1110	161	--	--	1482	215	--	--
PXA	PAW-GTA	4	X	Contractor X	A[b]	1096	159	1393	202	1344	195	1551	225
BNA	Base metal	2	--	NASA	A	1172	170	[c]1310	[c]190	1406	204	[c]1724	[c]250

[a]The heat-treatment prefix symbols are defined in the section entitled "Machining and Heat Treatment."

[b]Specimens heat treated by NASA at JSC. All other specimens heat treated by contractor Y.

[c]No test results. Value obtained from reference 2

TABLE VI.- TENSILE TEST RESULTS FOR WELDED AND BASE-METAL INCONEL 718 SPECIMENS

Specimen number	Test environment	Specimen thickness		Specimen width		Modulus, E		F_{TY}		F_{TU}	
		cm	in.	cm	in.	MN/m^2	ksi	MN/m^2	ksi	MN/m^2	ksi
GXA-1	RT[a] air	1.621	0.6383	1.585	0.6239	236×10^3	34.3×10^3	1220	177	1400	203
GXA-2	RT air	1.688	.6647	1.331	.5240	230	33.3	1103	160	1303	189
GNA-11	RT air	1.586	.6244	.7470	.2941	197	28.5	1082	157	1351	196
GNA-12	RT air	1.590	.6260	.7645	.3010	227	33.0	1186	172	1365	198
GNA-24	RT air	1.728	.6804	.5695	.2242	205	29.8	1089	158	1379	200
GNA-13	LN_2	1.587	.6250	.7526	.2963	(b)	(b)	(b)	(b)	1413	205
GNA-32	LN_2	1.686	.6638	.5458	.2149	223	32.3	1234	179	1613	234
GNB-21	RT air	1.699	.6688	.5187	.2042	211	30.6	1089	158	1317	191
GNB-22	RT air	1.729	.6810	.5425	.2136	218	31.6	965	140	1262	183
GNB-23	LN_2	1.705	.6711	.5804	.2285	254	36.9	1220	177	1530	222
GNC-31	RT air	1.663	.6549	.5618	.2212	208	30.1	1020	148	1310	190
GNC-32	RT air	1.671	.6580	.5514	.2171	207	29.1	1062	154	1275	185
GNC-33	LN_2	1.660	.6535	.5263	.2072	231	33.5	1227	178	1531	222
GYA-3	RT air	1.712	.6742	.5547	.2184	221	32.1	1055	153	1393	202
GYA-4	RT air	1.715	.6753	.5629	.2216	224	32.5	1027	149	1048	152
GYA-1	LN_2	1.710	.6732	.5395	.2124	270	39.1	1165	169	1641	238
GYA-2	LN_2	1.709	.6730	.5423	.2135	214	31.1	1248	181	1489	216
PXA-1	RT air	1.860	.7323	.5568	.2192	239	34.6	1096	159	1351	196
PXA-2	RT air	1.843	.7255	.5458	.2149	221	32.1	1089	158	1338	194
PXA-3	LN_2	1.856	.7306	.5314	.2092	239	34.7	1407	204	1600	232
PXA-4	LN_2	1.861	.7327	.4755	.1872	201	29.2	1379	200	1503	218
EXA-1	RT air	1.871	.7365	.5771	.2272	223	32.3	1103	160	1386	201
EXA-2	RT air	1.873	.7373	.5430	.2138	218	31.7	1117	162	1358	197
EXA-3	RT air	1.872	.7370	.4981	.1961	208	30.2	1089	158	1386	201
EXA-4	LN_2	1.873	.7375	.5463	.2151	(b)	(b)	(b)	(b)	1641	238
EXA-5	LN_2	1.873	.7374	.5088	.2003	(b)	(b)	(b)	(b)	1531	222
EXA-6	LN_2	1.877	.7390	.5375	.2116	214	31.0	1330	193	1455	211
ENA-1	RT air	1.763	.6940	.9627	.3790	203	29.4	1103	160	1600	232
ENA-2	RT air	1.770	.6970	.9627	3790	207	30.0	1124	163	1365	198
BNA-4	RT air	1.847	.7270	.9710	.3823	223	32.4	1165	169	1413	205
BNA-5	RT air	1.848	.7276	.9627	.3790	209	30.3	1172	170	1400	203

[a]RT = room temperature.

[b]Strain gage slipped.

TABLE VII.- VALUES OF Φ^2 AS A FUNCTION OF a/b

$$\left[\Phi = \int_0^{\frac{\pi}{2}} \left[1 - \left(\frac{b^2 - a^2}{b^2}\right)\sin^2\theta\right]^{\frac{1}{2}} d\theta\right]$$

a/b	Φ^2
0.00000	1.000000
.22361	1.124605
.31622	1.220527
.38729	1.307354
.44721	1.388838
.50000	1.466656
.54772	1.541746
.59161	1.614772
.63245	1.685915
.67082	1.755688
.70710	1.824239
.74162	1.891730
.77459	1.958297
.80622	2.024049
.83666	2.089074
.86602	2.153444
.89443	2.217225
.92195	2.280468
.94868	2.343220
.97468	2.405517
1.00000	2.467400

TABLE VIII. - SUMMARY OF AVERAGE TEST RESULTS FOR K_{IE}

Type of weld or metal	Specimen number prefix	Welding contractor	Base-metal source	Postweld heat treatment (a)	Average results for K_{IE}			
					Ambient air		LN_2	
					$MN/m^{3/2}$	ksi $\sqrt{in.}$	$MN/m^{3/2}$	ksi $\sqrt{in.}$
GTA	GTXA	X	Contractor X	A[b]	74	67	65	59
GTA	GTNA	X	NASA	A	89	81	82	75
GTA	GTNB	X	NASA	B	102	93	96	87
GTA	GTNC	X	NASA	C	81	74	68	62
GTA	GTYA	Y	NASA	A	79	72	79	72
EB	EBXA	X	Contractor X	A	54	49	38	35
EB	EBNA	X	NASA	A	74	67	60	55
PAW-GTA	PAXA	X	Contractor X	A[b]	58	53	53	48
Base metal	BANA	--	NASA	A	160	146	168	153

[a]The heat-treatment prefix symbols are defined in the section entitled "Machining and Heat Treatment."
[b]Specimens heat treated by NASA at JSC. All other specimens heat treated by contractor Y.

TABLE IX. - VALUE OF CONSTANTS IN EQUATION (7)

Type of weld or metal	Environment	S	K_{IE}		C_a		
			$MN/m^{3/2}$	ksi $\sqrt{in.}$	$\frac{nm/cycle}{(MN/m^{3/2})^{S-1}}$	$\frac{\mu in/cycle}{(ksi\sqrt{in.})^{S-1}}$	$\frac{in/cycle}{(psi\sqrt{in.})^{S-1}}$
GTA, heat treatment A	RT[a] air	3.7	89	81	0.000157	0.00113	0.9×10^{-17}
GTA, heat treatment A	LN_2	3.7	82	75	.000157	.00113	.9
GTA, heat treatment B	RT air	3.7	102	93	.000157	.00113	.9
GTA, heat treatment B	LN_2	3.7	96	87	.000157	.00113	.9
GTA, heat treatment C	RT air	3.7	81	74	.000157	.00113	.9
GTA, heat treatment C	LN_2	3.7	68	62	.000157	.00113	.9
Pulse GTA	RT air	3.7	79	72	.000157	.00113	.9
Pulse GTA	LN_2	3.7	79	72	.000157	.00113	.9
EB	RT air	3.7	74	67	.000471	.00339	2.7
EB	LN_2	3.7	60	55	.000471	.00339	2.7
PAW-GTA	RT air	3.7	58	53	.000314	.00226	1.8
PAW-GTA	LN_2	3.7	53	48	.000314	.00226	1.8
Base metal	RT air	3.7	160	146	.000026	.00018	.15
Base metal	LN_2	3.7	168	153	.000026	.00018	.15

[a]RT = room temperature.

JOINT CONFIGURATION

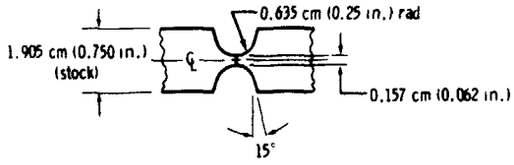

WELD PARAMETERS

Welding equipment: Linde semiautomatic welder with 300-A power supply, straight polarity
Process: GTA
Filler material: Inconel 718 wire, 0.102 cm (0.040 in.) diam
Shielding gas: Argon
Electrode: 2 percent thoriated tungsten, 0.397 cm (0.156 in.) diam
Cleaning: Wire brush and degrease with methylethylketone before each pass

Weld pass	Weld side	Potential, V	Current, A	Travel		Wire feed	
				cm/min	in/min	cm/min	in/min
1	1	12	80	20	8	53.3	21
2	2	12	90	20	8	53.3	21
3	1	12	150	20	8	63.5	25
4	2	12	180	20	8	63.5	25
5	1	12	180	20	8	102	40
6	2	12	180	20	8	102	40
7	1	12	180	20	8	102	40
8	2	12	180	20	8	147	58
9	1	12	180	20	8	147	58
10	2	12	180	20	8	147	58
11	1	12	180	20	8	147	58
12	2	12	180	20	8	147	58
13	1	12	180	20	8	147	58
14	2	12	180	20	8	147	58
15	1	12	160	20	8	102	40
16	2	12	160	20	8	102	40
17	1	12	140	20	8	102	40
18	2	12	140	20	8	102	40
19	1	12	140	20	8	102	40
20	2	12	140	20	8	102	40

Figure 1. - Joint configuration and weld parameters for GTA welds (GTXA-numbered fracture specimens).

JOINT CONFIGURATION

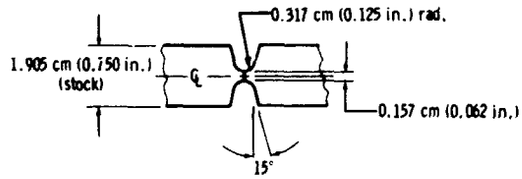

WELD PARAMETERS

Welding equipment: Linde semiautomatic welder with 300-A power supply, straight polarity
Process: GTA
Filler material: Inconel 718 wire, 0.102 cm (0.040 in.) diam
Shielding gas: Argon
Electrode: 2 percent thoriated tungsten, 0.397 cm (0.156 in.) diam
Cleaning: Rotary grind and degrease with methylethylketone before each pass

Weld pass	Weld side	Potential, V	Current, A	Travel		Wire feed	
				cm/min	in/min	cm/min	in/min
1	1	11	130	20	8	53.3	21
2	2	11	160	20	8	53.3	21
3	1	11	160	20	8	122	48
4	2	11	160	20	8	122	48
5	1	11	160	20	8	122	48
6	2	11	180	20	8	122	48
7	1	11	185	20	8	122	48
8	2	11	190	20	8	122	48
9	1	11	190	20	8	122	48
10	2	11	190	20	8	122	48
11	1	11	170	20	8	122	48
12	2	11	170	20	8	122	48
13	1	11	180	20	8	147	58
14	2	11	180	20	8	147	58
15	1	11	160	20	8	53.3	21
16	2	11	160	20	8	53.3	21

Figure 2. - Joint configuration and weld parameters for GTA welds (GTNA-, GTNB-, and GTNC-numbered fracture specimens).

JOINT CONFIGURATION

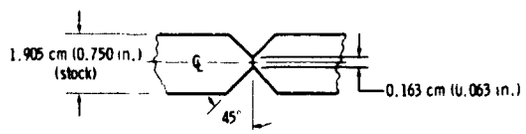

WELD PARAMETERS

Welding equipment	Dimetrics Hi-Pulse 400
Process:	Pulse GTA
Filler material.	Inconel 718 wire, 0.076 cm (0.030 in.) diam
Shielding gas.	Argon
Electrode:	2 percent thoriated tungsten, 0 317 cm (0.125 in.) diam
Clearing:	Wire brush and degrease with methylethylketone before each pass

Weld pass	Weld side	Potential, V	Current, A	Wire feed		Frequency, kHz	Travel	
				cm/min	in/min		cm/min	in/min
1	1	10.0	170	0	0	22.5	8.25	3.25
2	1	10.0	130	76	30	22.5	11.4	4.5
3	2	10 0	130	0	0	22.5	11.4	4.5
4	2	10.5	145	114	45	22.5	12.7	5.0
5	2	10.5	145	114	45	22.5	12.7	5.0
6	1	10.5	145	114	45	22 5	12.7	5.0
7	1	10 5	145	114	45	22.5	12.7	5.0
8	1	10.5	145	114	45	22.5	12.7	5.0
9	2	10 5	145	114	45	22.5	12.7	5.0
10	2	10.5	145	114	45	22.5	12.7	5.0
11	2	10.5	145	114	45	22.5	12.7	5.0
12	1	10.5	145	114	45	22.5	12.7	5.0
13	1	10.5	145	114	45	22 5	12.7	5.0
14	1	10.5	145	114	45	22.5	12.7	5.0
15	2	10.5	145	114	45	22.5	12.7	5.0
16	2	12.0	145	152	60	22.5	15.2	6.0
17	2	12.0	145	152	60	22.5	15.2	6.0
18	1	12.0	145	152	60	22.5	15.2	6.0
19	1	12.0	145	152	60	22.5	15.2	6.0
20	1	12.0	145	152	60	22.5	15 2	6.0
21	2	12.0	145	152	60	22.5	15 2	6 0

Figure 3. - Joint configuration and weld parameters for pulse GTA welds (GTYA-numbered fracture specimens).

JOINT CONFIGURATION

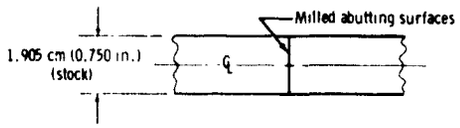

WELD PARAMETERS

Welding equipment	Sciaky electron-beam welder with 500-mA beam current at 60 000 V maximum accelerating potential
Process:	EB
Shielding:	Vacuum chamber
Cleaning:	Degrease with methylethylketone and subsequent pickle

Weld pass	Potential, V	Current, mA	Travel		Weld width, cm (in.)	
			cm/min	in/min	Top	Bottom
Seal	43 000	60	61.0	24	--	--
Penetration	43 000	330	61.0	24	0.25 (0.10)	0 13 (0 05)
Cosmetic	20 000	40	30.5	12	--	--

Figure 4. - Joint configuration and weld parameters for EB welds (EBXA- and EBNA-numbered fracture specimens).

REPRODUCIBILITY OF THE ORIGINAL PAGE IS POOR.

JOINT CONFIGURATION

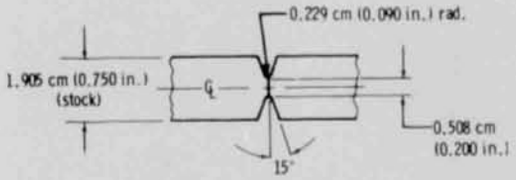

WELD PARAMETERS

Welding equipment:	GTA - Linde semiautomatic welder with 300-A power supply, straight polarity PAW - 400-A Linde power supply on Linde GTA equipment
Process:	PAW root penetration and GTA fill
Filler material:	Inconel 718 wire, 0.114 cm (0.045 in.) diam
Shielding gas:	90 percent argon and 10 percent hydrogen for PAW; argon for GTA welds
Electrode:	2 percent thoriated tungsten, 0.317 cm (0.125 in.) diam for PAW; 0.397 cm (0.156 in.) diam for GTA welds
Cleaning:	Wire brush and degrease with methylethylketone before each pass

Weld pass	Weld side	Type weld	Potential, V	Current, A	Travel		Wire feed	
					cm/min	in/min	cm/min	in/min
1	1	PAW	22.5	225	30.5	12	0	0
2	2	GTA	24	190	20.3	8	76.2	30
3	1	GTA	24	190	20.3	8	180	71
4	2	GTA	24	190	20.3	8	180	71
5	1	GTA	24	190	20.3	8	180	71
6	2	GTA	24	190	20.3	8	180	71
7	1	GTA	24	190	20.3	8	180	71
8	2	GTA	24	190	20.3	8	180	71
9	1	GTA	24	190	20.3	8	180	71

Figure 5. - Joint configuration and weld parameters for PAW-GTA welds (PAXA-numbered fracture specimens).

(a) GTA weld.

(b) PAW-GTA weld.

Figure 6. - Section photographs of GTA weld and PAW-GTA weld.

REPRODUCIBILITY OF THE ORIGINAL PAGE IS POOR.

(a) Weld with complete fusion at root.

(b) Weld with incomplete fusion at root.

Figure 7. - Section photographs of pulse GTA weld.

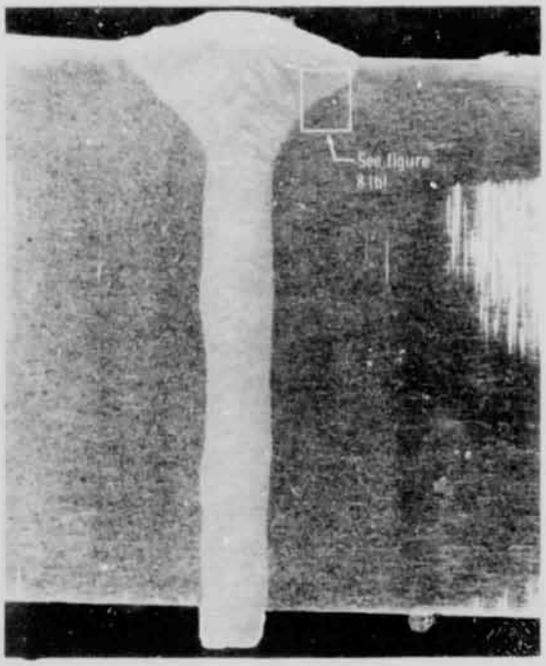

(a) Full section photograph.

(b) A 100× enlargement showing microfissure cracks in heat-affected zone.

Figure 8. - Section photographs of EB weld.

REPRODUCIBILITY OF THE ORIGINAL PAGE IS POOR.

(a) Section view of weld.

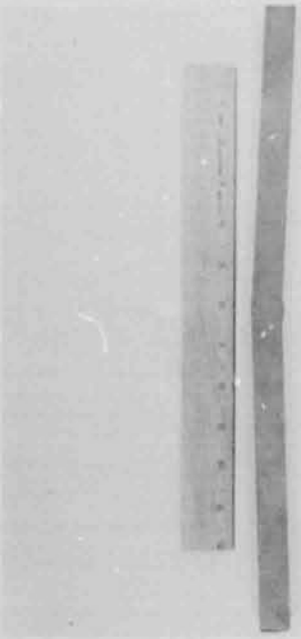

(b) Edge view showing warpage (scale in inches).

Figure 9. - Photographs of PAW welded plate.

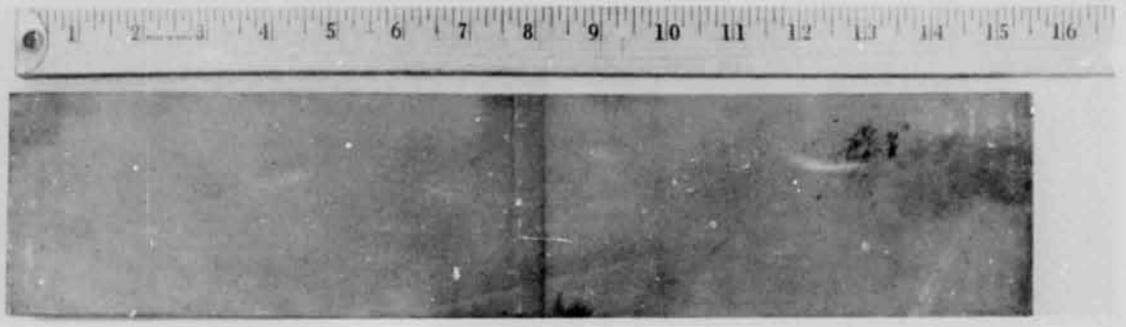

(a) Weld specimen after heat treatment (scale in inches).

(b) Weld specimen after machining.

Figure 10. - Photograph of typical weld specimens after heat treatment and final machining.

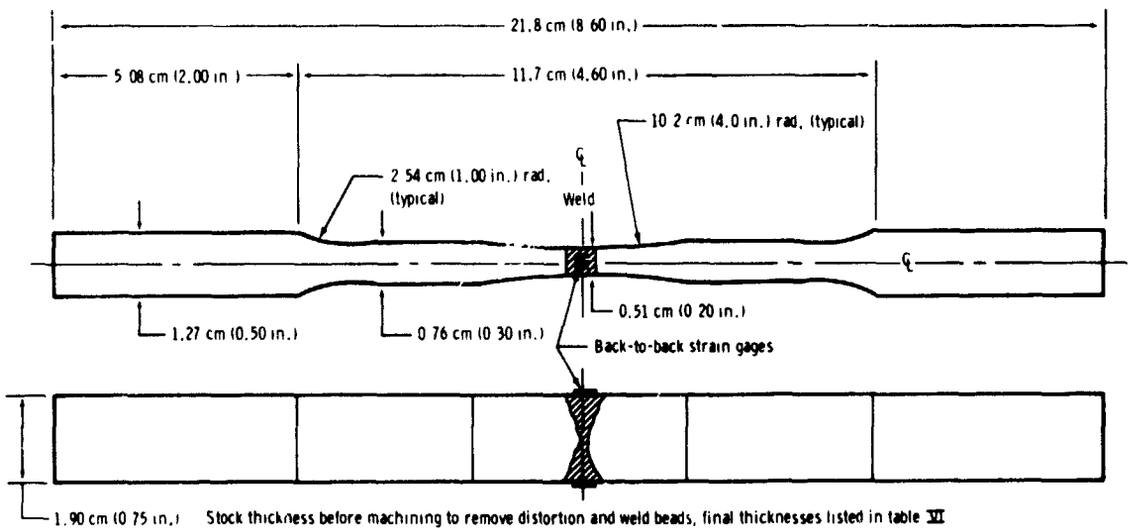

Figure 11. - Typical tensile specimen configuration.

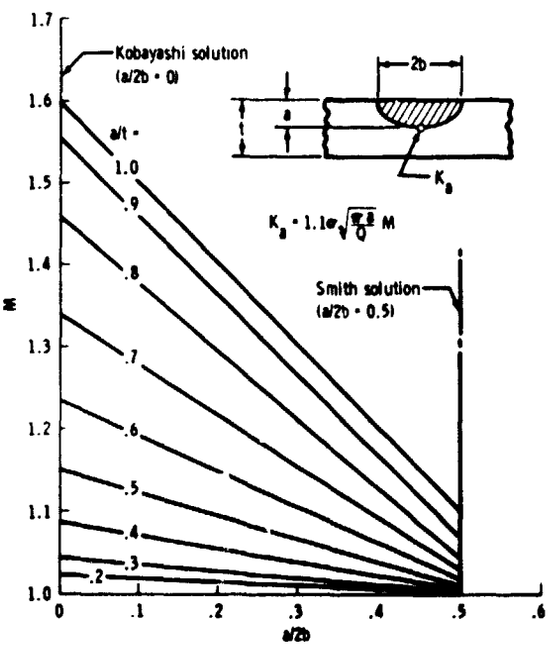

Figure 12. - Determination of deep-flaw magnification factor M.

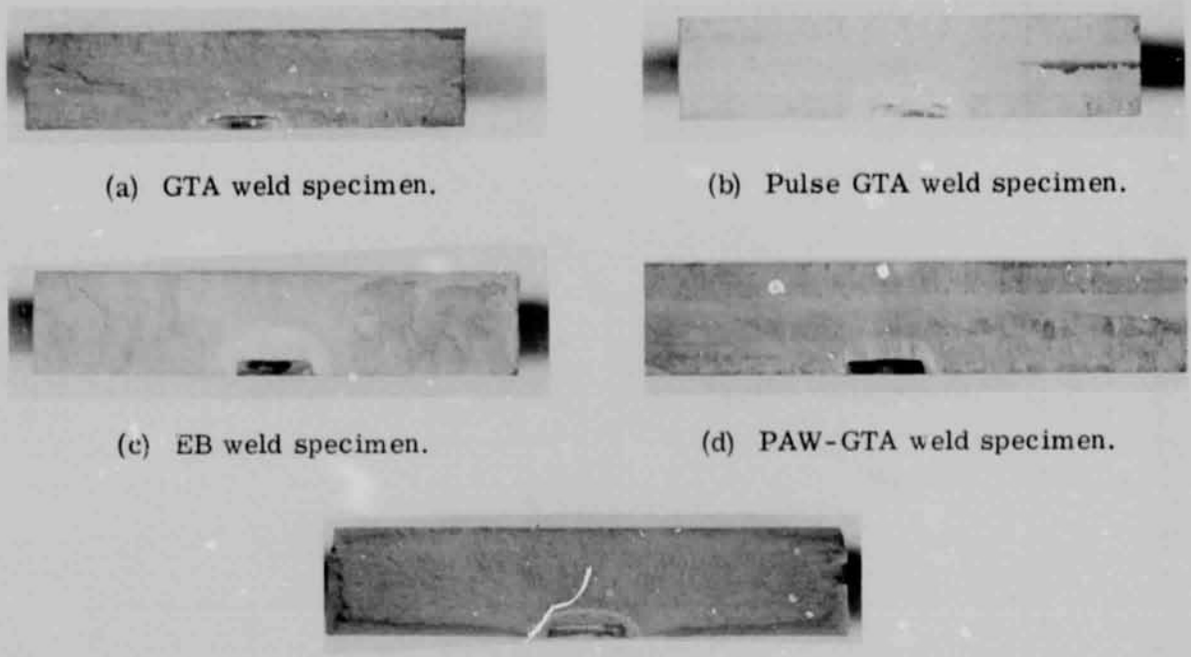

(a) GTA weld specimen.

(b) Pulse GTA weld specimen.

(c) EB weld specimen.

(d) PAW-GTA weld specimen.

(e) Base-metal specimen.

Figure 13. - Fracture face photographs of fatigue-cracked specimens.

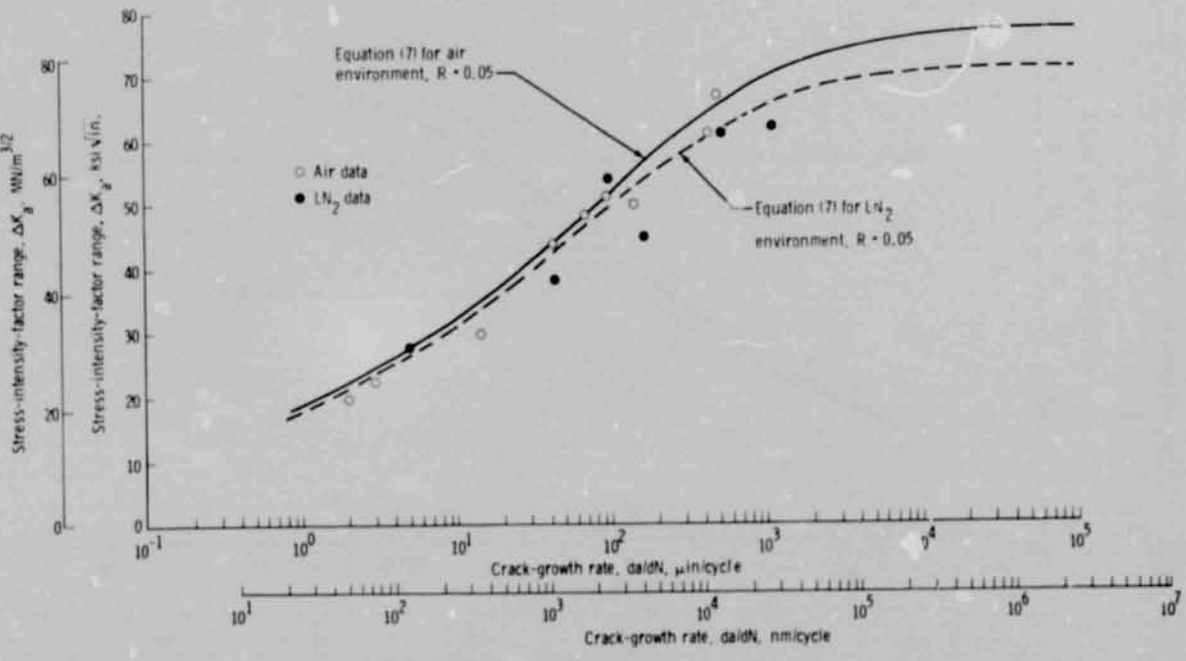

Figure 14. - Comparison of theoretical crack-growth rate with experimental data from GTA welds, heat treatment A.

REPRODUCIBILITY OF THE ORIGINAL PAGE IS POOR.

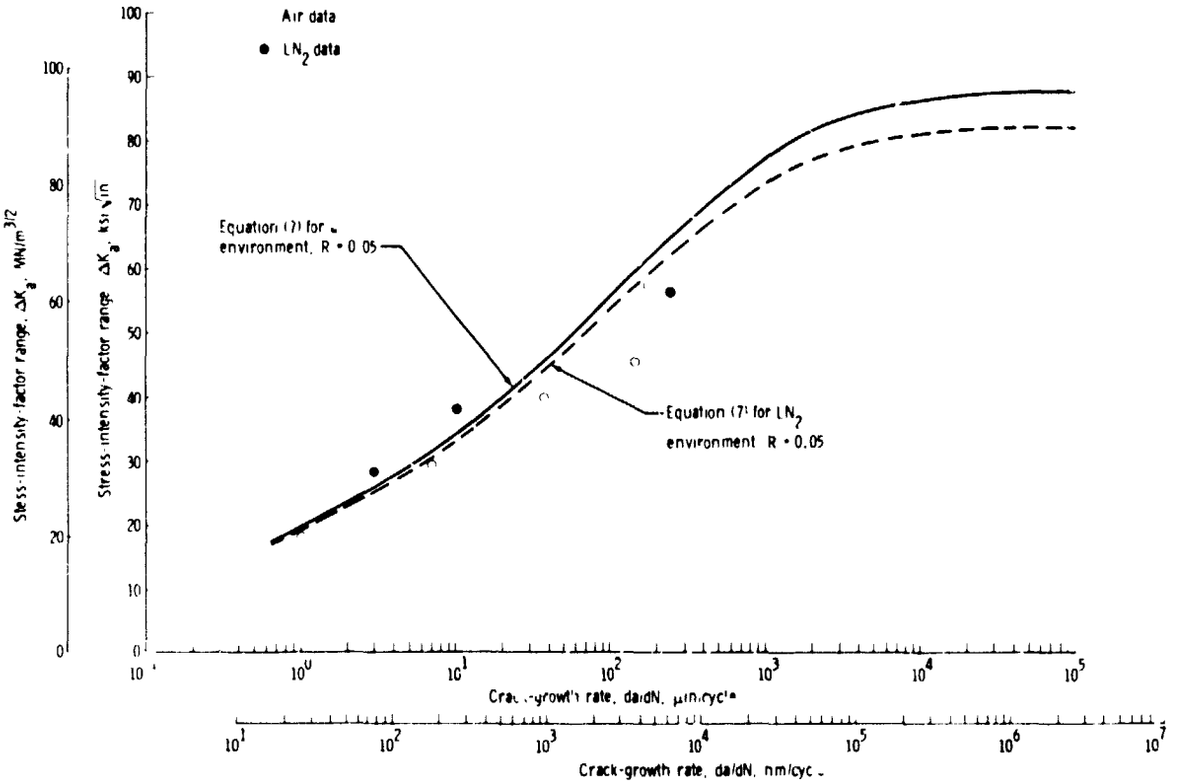

Figure 15. - Comparison of theoretical crack-growth rate with experimental data from GTA welds, heat treatment B.

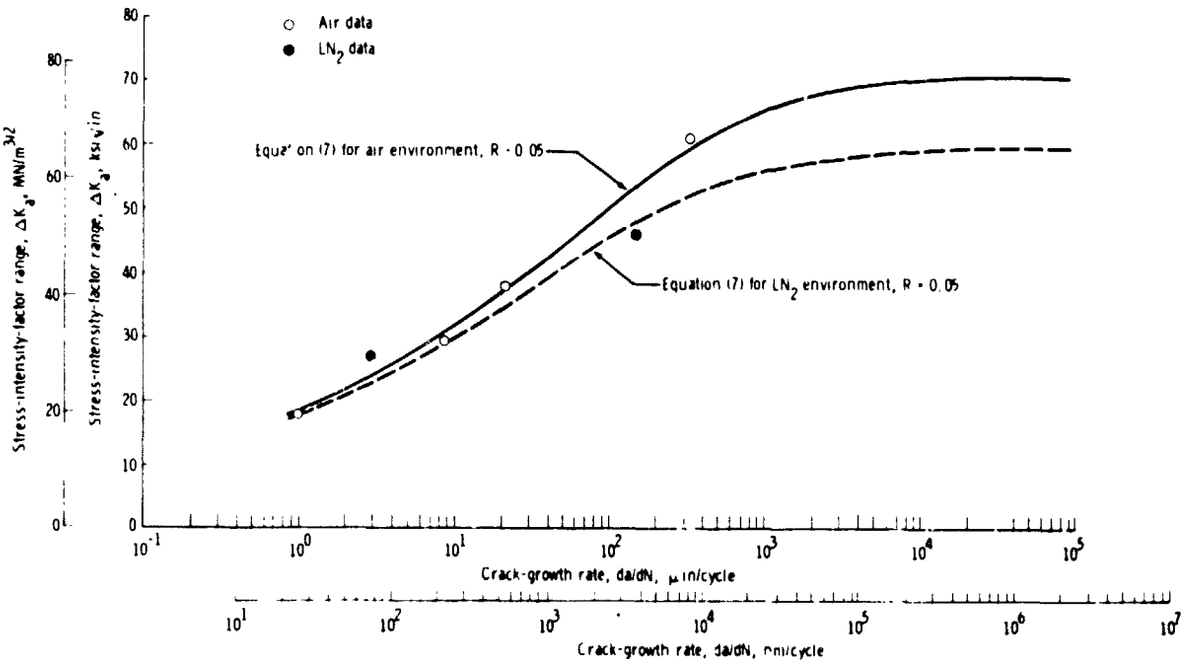

Figure 16. - Comparison of theoretical crack-growth rate with experimental data from GTA welds, heat treatment C.

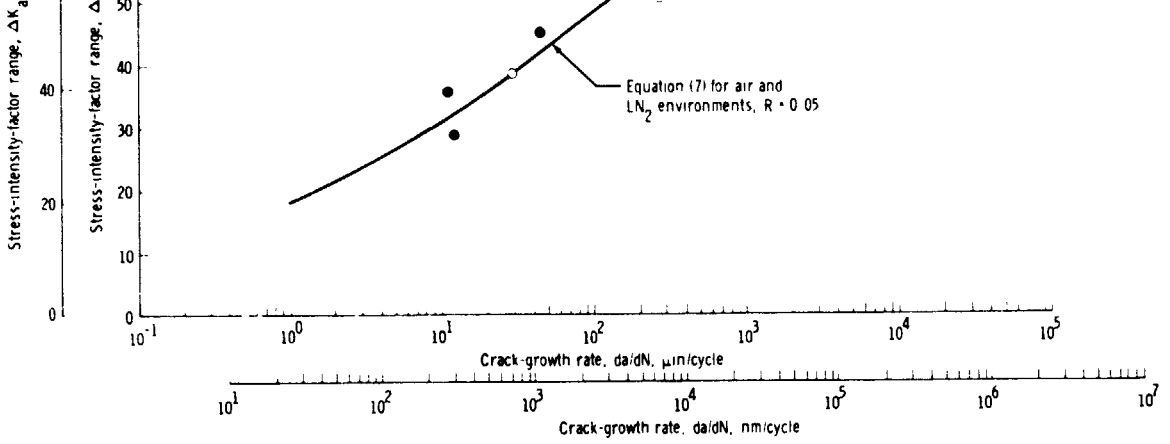

Figure 17. - Comparison of theoretical crack-growth rate with experimental data from pulse GTA welds, heat treatment A.

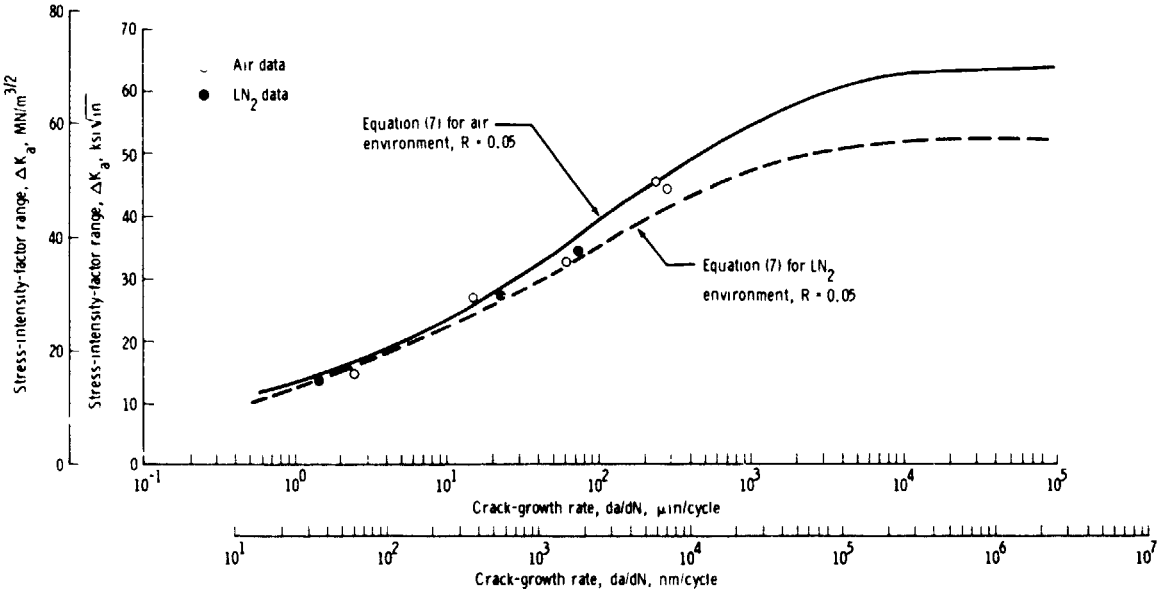

Figure 18. - Comparison of theoretical crack-growth rate with experimental EB weld data.

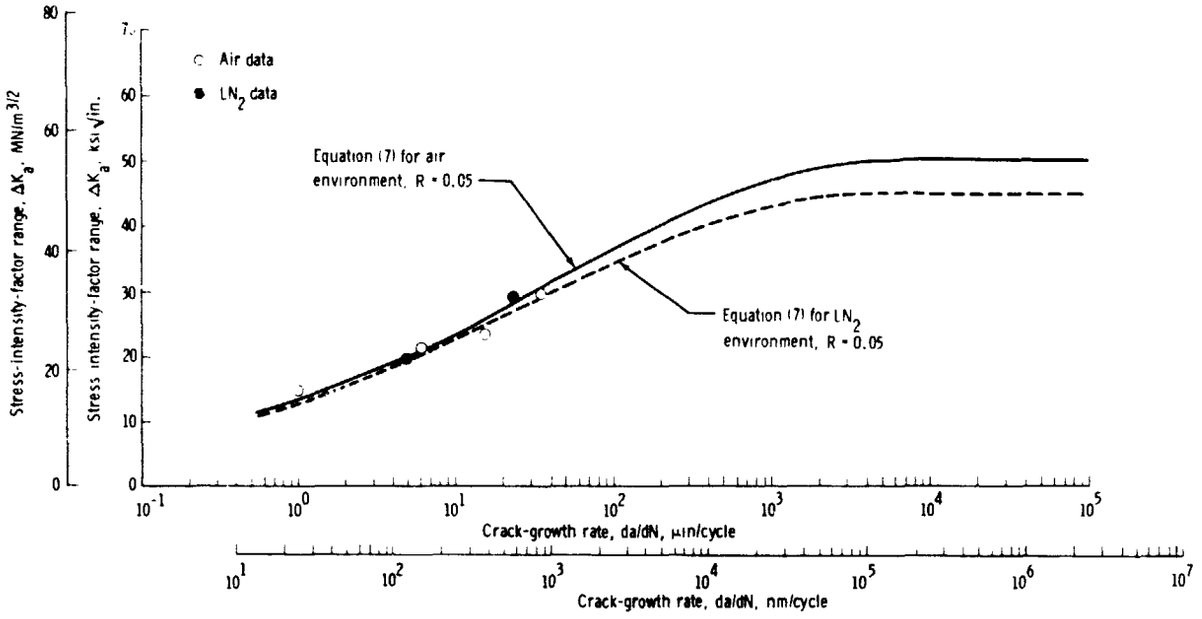

Figure 19. - Comparison of theoretical crack-growth rate with experimental PAW-GTA weld data.

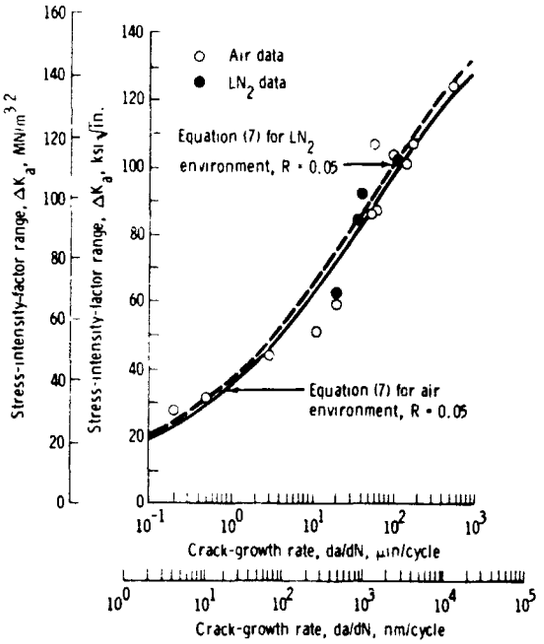

Figure 20. - Comparison of theoretical crack-growth rate with experimental base-metal data.

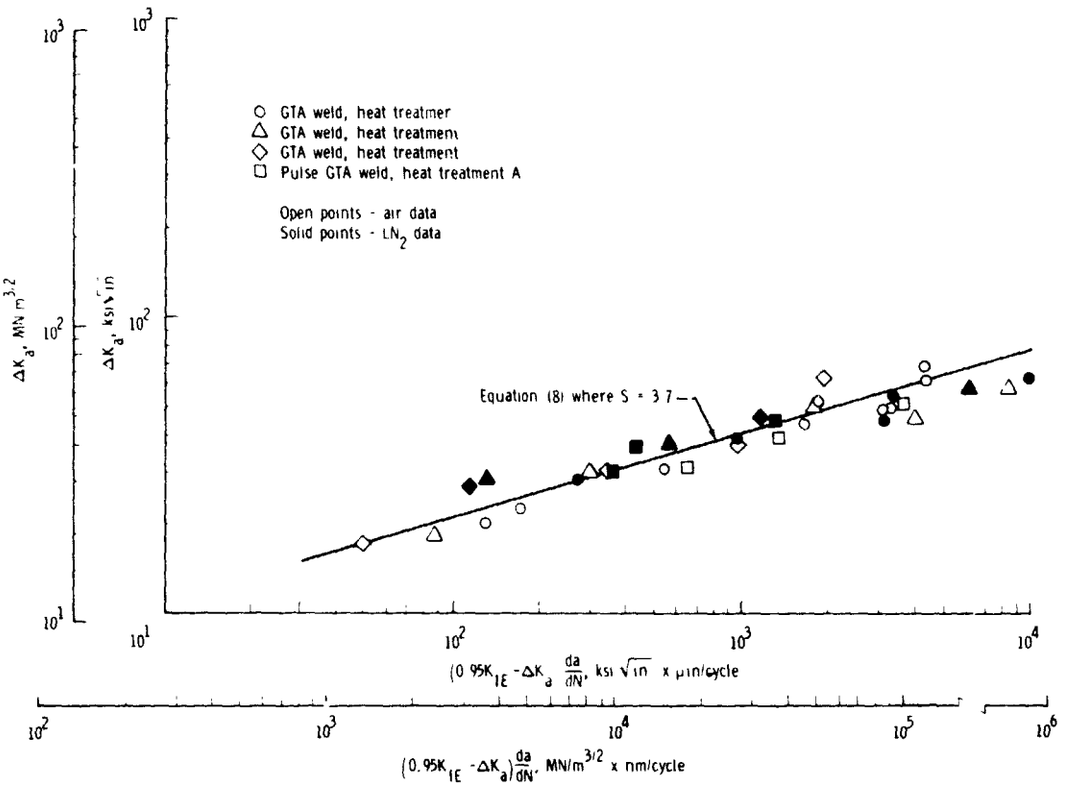

Figure 21. - Comparison of theoretical crack-growth rate (linearized) with experimental GTA and pulse GTA weld data.

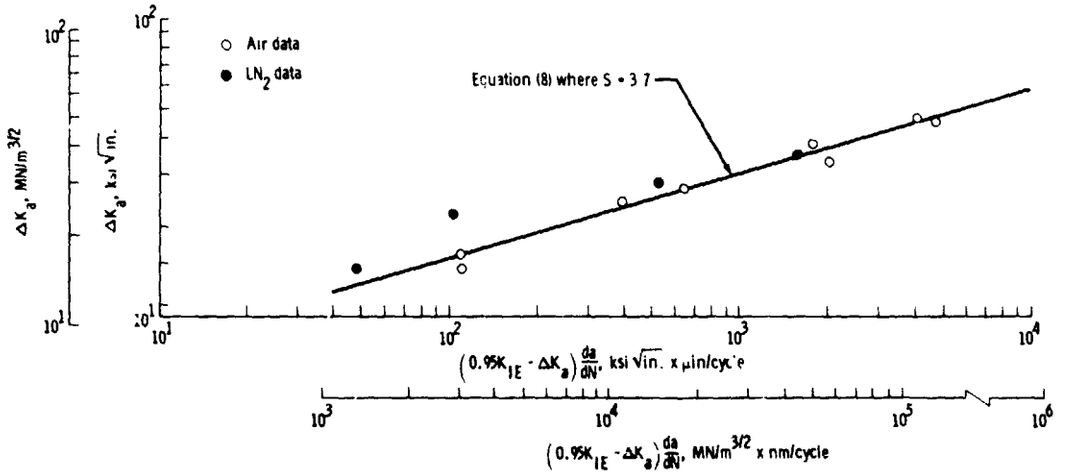

Figure 22. - Comparison of theoretical crack-growth rate (linearized) with experimental EB weld data.

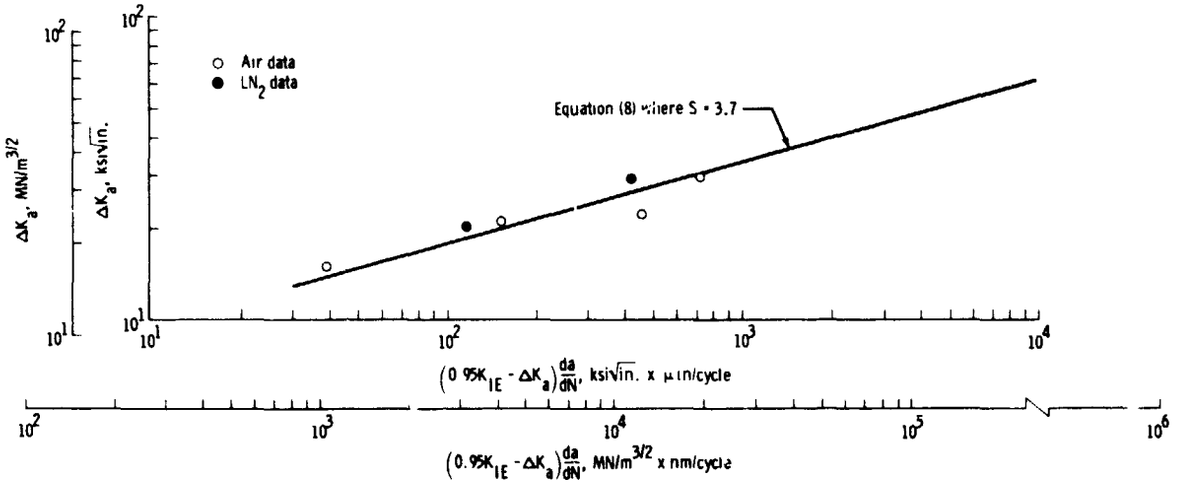

Figure 23. - Comparison of theoretical crack-growth rate (linearized) with experimental PAW-GTA weld data.

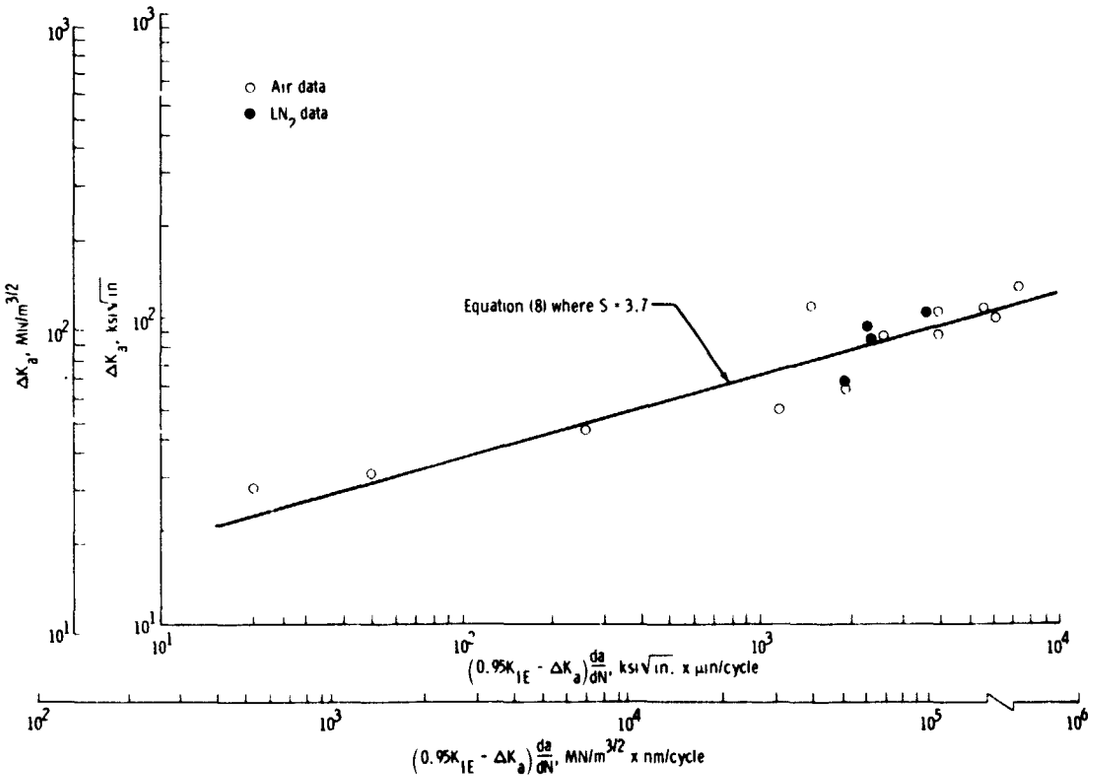

Figure 24. - Comparison of theoretical crack-growth rate (linearized) with experimental base-metal data.

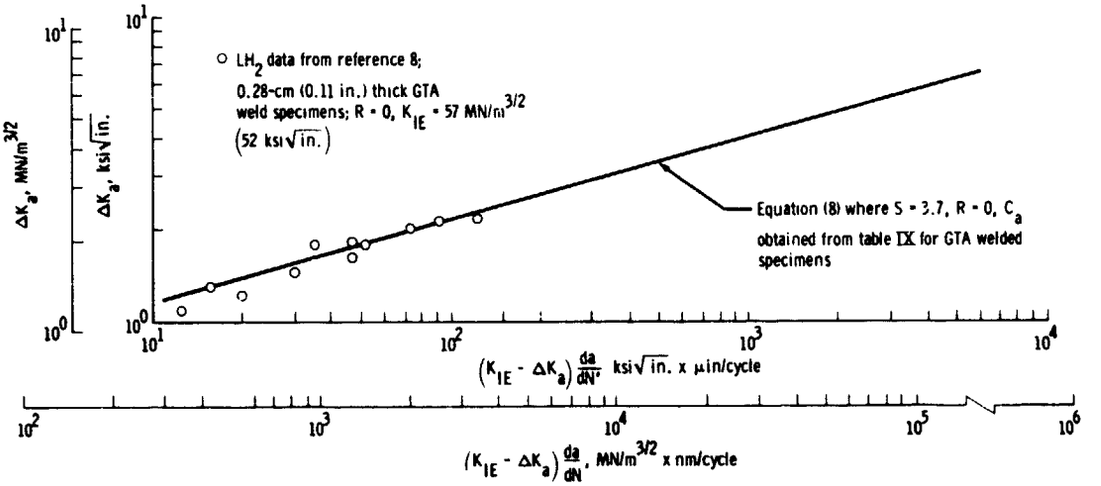

Figure 25. - Comparison of theoretical crack-growth rate (linearized) with liquid hydrogen (LH_2) temperature GTA weld data from reference 8.

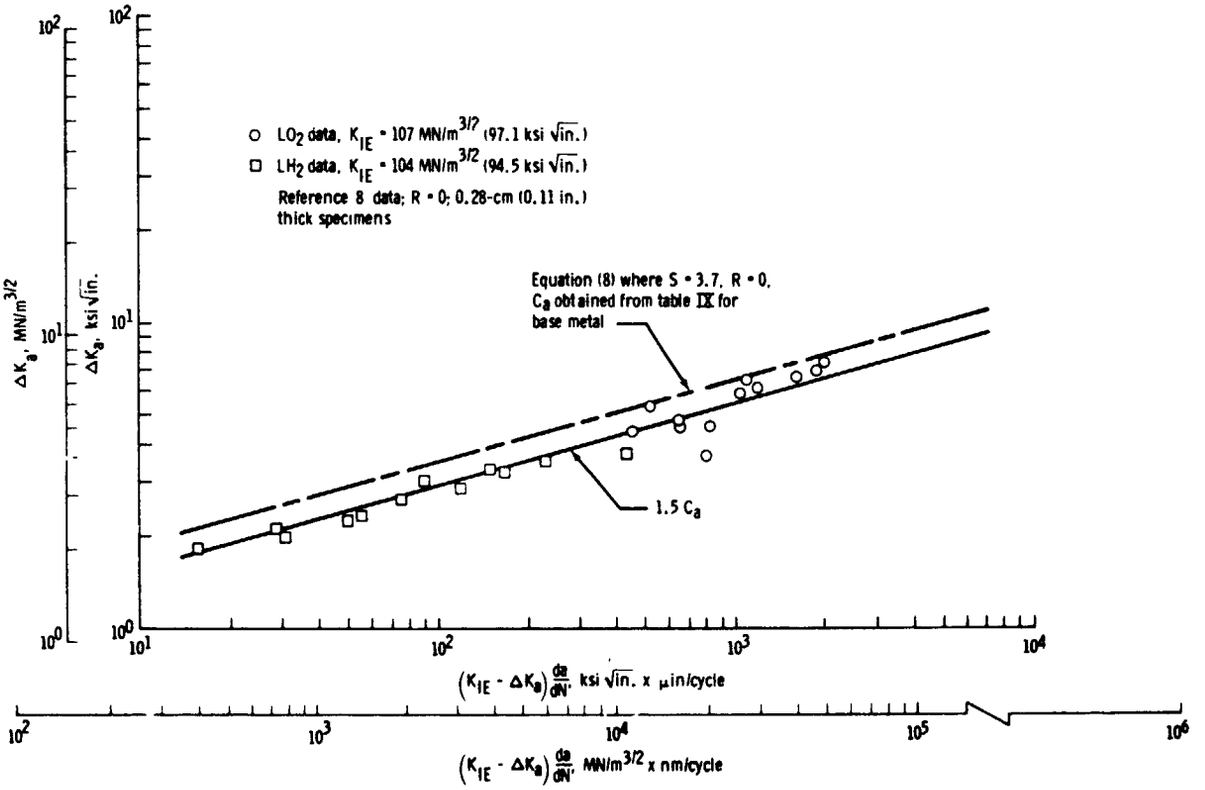

Figure 26. - Comparison of theoretical crack-growth rate (linearized) with liquid oxygen (LO_2) and LH_2 temperature base-metal data from reference 8.

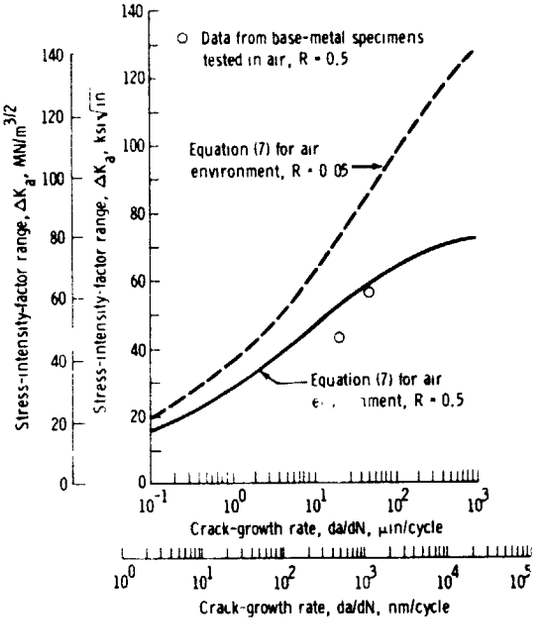

Figure 27. - Comparison of theoretical crack-growth rate with base-metal experimental data for R = 0.5.

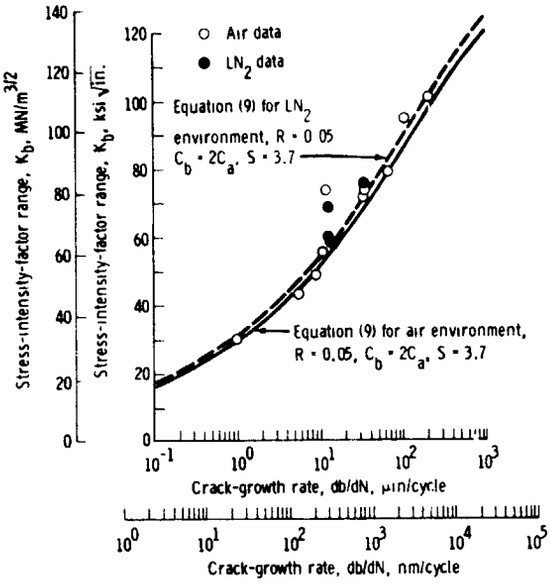

Figure 28. - Comparison of theoretical crack-growth rate on the specimen surface with experimental base-metal data.

APPENDIX

CONVERSION OF U.S. CUSTOMARY UNITS TO SI UNITS

The Système International d'Unités (SI) was adopted by the Eleventh General Conference on Weights and Measures in Paris during October 1960, in Resolution Number 12. The factors required for conversion of U.S. customary units used in this report to SI units and the prefixes and symbols used to indicate multiples of units are presented in the following tables.

To convert from U.S. customary units	Multiply by —	To obtain SI units
lbf	4.448222	newtons (N)
in.	2.54×10^{-2}	meters (m)
kips per square inch (ksi)	6.894757×10^{-6}	newtons/meter^2 (N/m^2)
ksi $\sqrt{in.}$	1.0988	$MN/m^{3/2}$
μin/cycle	25.4	nm/cycle

Multiple	Prefix	Symbol
10^{-9}	nano	n
10^{-6}	micro	μ
10^{-3}	milli	m
10^{6}	mega	M
10^{9}	giga	G